Zika virus-induced fetal demise is driven by strain- and dose-specific RLR-driven activation of the interferon response in the decidua, placenta, and fetus in *Ifnar1*$^{-/-}$ mice.

Ellie K. Bohm[1], David Castañeda[1], Qun Lu[2], Michael D. Cameron[2], Matthew T. Aliota[1#]

[1]Department of Veterinary and Biomedical Sciences, University of Minnesota, Twin Cities, St. Paul, MN 55455, USA.

[2]The Herbert Wertheim UF Scripps Institute for Biomedical Innovation and Technology, Jupiter, FL, United States.

#Correspondence: mtaliota@umn.edu

ABSTRACT

Congenital Zika syndrome (CZS), the set of fetal and neonatal complications associated with Zika virus (ZIKV) infection in pregnancy, was first noted during the outbreak in the Americas in 2015-16. However, there was an unequal distribution of ZIKV cases and severe outcomes in all areas where ZIKV emerged in the Americas, demonstrating that the risk of CZS varied over space and time. Recently, we demonstrated that phenotypic heterogeneity existed between closely-related ZIKV strains. All ZIKV strains tested infected the placenta but varied in their capacity to cause overt fetal harm. Here, we further characterized the relative contributions of virus genotype and infecting dose of two phenotypically distinct ZIKV strains across multiple timepoints in gestation in pregnant mice that lack type-I interferon receptor function (*Ifnar1*$^{-/-}$). To better understand the underlying causes of adverse fetal outcomes, we used RNA sequencing to compare ZIKV-infected and uninfected tissues. We found that ZIKV infection triggers retinoic acid-inducible gene I (RIG-I)-like receptor-mediated activation of the interferon response at the maternal-fetal interface. However, modest chemical inhibition of RIG-I activation in the decidua and placenta did not protect against fetal demise. Instead, the fetal interferon response was significantly associated with fetal demise. Together, these findings suggest that the response to

ZIKV at the maternal-fetal interface can vary depending on the infecting ZIKV genotype and dose, and that the fetal immune response is an important mediator of fetal harm.

IMPORTANCE

Previously, we used a mouse model of ZIKV infection during pregnancy to assess the pathogenic potential to the fetus of a panel of five, low-passage ZIKV strains representing the viral genetic diversity in the Americas. We found that phenotypic heterogeneity existed between these closely-related ZIKV strains. Here, we show that this heterogeneity is driven by retinoic acid-inducible gene I (RIG-I)-like receptor-mediated activation of the interferon response at the maternal-fetal interface. We used chemical inhibition of the RIG-I pathway and measured the transcriptional activity of interferon stimulated genes in fetuses to demonstrate that the fetal immune response may contribute to fetal demise.

INTRODUCTION

Zika virus (ZIKV) infection during pregnancy can cause a spectrum of adverse fetal outcomes collectively termed Congenital Zika Syndrome (CZS), but not all children exposed to ZIKV *in utero* develop these abnormalities. While it is well-established that ZIKV can cause fetal harm, *how* ZIKV causes fetal harm remains unclear. Whether fetal pathology manifests for a given pregnancy is dependent on myriad factors including gestational age of the fetus, maternal immunity, maternal-fetal barrier integrity, and ZIKV tropism (1, 2). ZIKV can be vertically transmitted through the maternal-fetal barrier, but the route and frequency of transmission remains uncertain. It is thought that ZIKV is vertically transmitted from maternal circulation to the maternal-derived decidua, then to the adjacent fetal-derived placenta, and finally to the fetus (3, 4). ZIKV can replicate in several cell types of the human maternal-fetal interface (MFI) including maternal decidual cells (5), fetal trophoblast cells, and fetal endothelial cells (3). Many studies report detection of viral proteins and/or viral RNA (vRNA) in the placental tissues of ZIKV-infected pregnant people (6). Many animal studies recapitulate these findings with ZIKV vRNA detected in multiple MFI tissues of non-human primates (7, 8), but these same studies were unable to determine the route of transmission through the tissues. Human cohort studies report varying frequencies of infection of the MFI and fetus. In one case study, over half of ZIKV-infected mothers had ZIKV vRNA detected in placental and/or fetal tissue at term (9). In cases of severe microcephaly, evidence of fetal infection was relatively common (10–12), indicating that fetal infection is likely one mechanism of fetal harm. But with limited screening of apparently-normal infants who have subtle neurological sequelae, it remains unknown if fetal infection is a precursor in all cases of CZS.

Ultimately, fetal infection may not be required for fetal harm. Recent cohort studies show that infants with CZS have high levels of inflammatory markers (13, 14), suggesting a significant inflammatory response before birth. A robust inflammatory response can cause placental

dysfunction, a syndrome during which the placenta fails to develop properly and deliver nutrients, blood, and oxygen to the growing fetus. Placental dysfunction results in intrauterine growth restriction, abnormal development, and miscarriage (15), which have been observed in neonates and infants with CZS. ZIKV vRNA persistence at the MFI can also induce high levels of interferon (IFN) (16). In some animal models, placental damage caused by the IFN response was a precursor to fetal demise, and fetal infection was not required (17–21). Consistent with this, certain nucleotide polymorphisms in IFN receptors and immune profiles were associated with higher levels of IFN-stimulated genes and increased risk of CZS in humans (22, 23). Together, these findings suggest that ZIKV infection of the fetus is not required in all cases of fetal harm.

Epidemiological data from the 2015-2016 American outbreak showed that although Asian/American-lineage ZIKV strains share >99% nucleotide-identity (24), they cause heterogeneous rates of fetal harm (25–31). This suggests ongoing virus evolution during the 2015-2016 outbreak in the Americas may have given rise to phenotypic variants that differ in the mechanism by which developing fetuses are harmed. Indeed, we unexpectedly found that phenotypic heterogeneity existed between closely-related ZIKV strains in a pregnant *Ifnar1*$^{-/-}$ mouse model (18). The Asian-lineage ZIKVs we tested had varying capacities to cause fetal demise, ranging between 9 - 51%—importantly, demise occurred in the absence of detectable fetal infection(18). Other infection parameters, including maternal viremia, placental infection, placental histopathology, and intrauterine growth restriction were similarly heterogeneous in our mouse model (18). Surprisingly, none of these phenotypes positively correlated with the rate of fetal demise.

Therefore, to identify other factors that may contribute to ZIKV-induced fetal demise, we leveraged the natural variability in phenotype that exists between closely-related ZIKV strains and initiated transcriptome profiling studies to assess gene expression changes in the placenta.

We used two ZIKV strains that showed different pregnancy phenotypes: a strain from Brazil, ZIKV-BRA (Paraiba_01), that causes significant fetal demise, and a strain from Mexico, ZIKV-MEX (R116265), that does not. We found that ZIKV infection results in strain- and dose-dependent activation of the IFN response at the MFI prior to fetal demise. Further analysis suggested that retinoic acid-inducible gene I (RIG-I) sensing of ZIKV vRNA was a primary driver of the IFN response. Since the IFN response is known to be pathogenic during pregnancies (17, 21), we aimed to investigate if chemical inhibition of RIG-I signaling reduced rates of fetal demise following ZIKV-BRA infection. We found that modest RIG-I inhibition at the MFI does not protect against fetal demise, but identified a strong association between an increased fetal IFN response and fetal demise.

RESULTS

ZIKV strain- and dose-dependent pregnancy phenotypes are present across gestation. Previously, we determined that there is strain-dependent phenotypic heterogeneity in pregnancy outcomes following *in utero* ZIKV exposure in pregnant *Ifnar1*$^{-/-}$ mice (18). We compared a panel of five geographically-distinct, low-passage Asian/American-lineage ZIKV strains and assessed pregnancy outcomes at a single necropsy timepoint (E14.5) to evaluate the extent to which pregnancy outcomes varied by infecting ZIKV genotype. Viruses from Brazil and Cambodia caused significantly more embryo resorption than viruses from Panama, Puerto Rico, and Mexico (18). Now, to determine when strain-dependent outcomes manifest and assess the influence of dose, we compared pregnancy outcomes at multiple points in gestation. We inoculated with 10^3 PFU ZIKV-MEX, 10^5 PFU ZIKV-MEX, and 10^3 PFU ZIKV-BRA. We chose these two ZIKV strains because they have distinct pregnancy phenotypes—ZIKV-BRA causes significant fetal resorption and ZIKV-MEX does not—when inoculated with 10^3 PFU (18). These virus strains differ by only seven amino acids (**Table 1**). We included a high-dose inoculation of ZIKV-MEX (10^5 PFU ZIKV-MEX) to determine if increasing the dose for this virus strain impacts the rate of fetal resorption. To assess pregnancy outcomes, *Ifnar1*$^{-/-}$ dams were time-mated with wildtype (WT) males to produce fetal and placental tissue with intact IFN signaling, as we have done previously (18, 19, 32). Pregnant *Ifnar1*$^{-/-}$ dams then were inoculated with 10^3 or 10^5 PFU ZIKV-MEX or 10^3 PFU ZIKV-BRA via subcutaneous footpad inoculation at embryonic day 7.5 (E7.5). E7.5 corresponds to the mid-to-late first trimester in humans (33). Dams were monitored daily for clinical signs until the time of necropsy; no overt clinical signs were observed in any virus- or PBS-inoculated dams. We collected serum at 2, 4, 7 (10^5 PFU ZIKV-MEX only), and 10 days post inoculation (dpi) to compare maternal viremia kinetics between the two viruses. At 2 dpi, all groups were significantly different from each other ($p < 0.0409$), with 10^5 PFU ZIKV-MEX-inoculated animals having the highest serum titers (**Figure 1A**). At 4 dpi, the 10^3 PFU

ZIKV-BRA group had significantly higher titers than both ZIKV-MEX groups ($p < 0.0001$). At 10 dpi, titers did not differ significantly between 10^3 PFU ZIKV-MEX, 10^5 PFU ZIKV-MEX, and 10^3 PFU ZIKV-BRA, and were largely undetectable. There was no significant difference between 10^5 PFU ZIKV-MEX and 10^3 PFU ZIKV-MEX and 10^3 PFU ZIKV-BRA from reference (Bohm 2021) at 7 dpi ($p > 0.9999$).

BRA	MEX	Protein	Codon
G	**A**	NS1	100
K	**E**	NS1	326
V	M	NS1	349
V	**I**	NS3	40
F	S	NS3	356
M	**L**	NS3	572
I	**T**	NS5	526

Table 1: Amino acid differences between ZIKV-MEX and ZIKV-BRA. Bold text indicates deviation from other Asian-lineage ZIKVs examined in reference (Bohm 2021).

Next, to compare the range of fetal outcomes across gestation, we necropsied dams on E11.5, E14.5, or E17.5. In an effort to minimize the use of animals, data for E14.5 for the 10^3 PFU ZIKV-MEX and 10^3 PFU ZIKV-BRA groups are derived from reference (18) and presented here for comparisons only. Gross examination of each conceptus revealed overt differences among fetuses within pregnancies, with uninfected counterparts, and across gestation. Fetuses appeared as either morphologically normal or undergoing embryo resorption, as defined in reference (19). The proportion of resorbed fetuses for 10^3 PFU ZIKV-MEX, 10^5 PFU ZIKV-MEX, and 10^3 PFU ZIKV-BRA-infected animals did not significantly differ from PBS-inoculated controls at E11.5 (Fisher's exact test, $p > 0.1338$)(**Figure 1B**). At E14.5, dams infected with 10^5 PFU ZIKV-MEX exhibited significant fetal resorption compared to PBS-inoculated controls and 10^3 PFU ZIKV-MEX (Fisher's exact test, $p < 0.0004$) and this rate of resorption was similar to the

rate caused by 10^3 PFU ZIKV-BRA in reference (18)(**Figure 1B**). The proportion of resorbed fetuses at E14.5 for 10^5 PFU ZIKV-MEX and 10^3 PFU ZIKV-BRA groups was also significantly higher than what was observed at E11.5 (Fisher's exact test, $p < 0.0001$)(**Figure 1B**), indicating that fetal resorption becomes grossly detectable between E11.5 and E14.5. At E17.5, the closest point to term that can be assessed in our model, the proportion of resorbed fetuses in 10^3 PFU ZIKV-MEX-infected animals remained no different from our PBS control group (Fisher's exact test, $p > 0.0856$)(**Figure 1B**), demonstrating that infection with 10^3 PFU ZIKV-MEX does not result in significant fetal resorption at any point across gestation. Infection with 10^3 PFU ZIKV-BRA, on the other hand, had high rates of fetal resorption at E14.5 and E17.5 that were significantly higher than PBS at all points assessed (Fisher's exact test, $p < 0.0128$) but were no different from each other (Fisher's exact test, $p = 0.0875$)(**Figure 1B**). The rate of fetal resorption varied significantly between individual pregnancies within each treatment group. Most groups had modest variation, but 10^5 PFU ZIKV-MEX and 10^3 PFU ZIKV-BRA displayed high variability at E14.5 and E17.5, ranging between 9 - 100%(**Figure 1C**).

We measured crown-to-rump length (CRL) at E11.5 and E17.5 to assess the impacts of ZIKV infection on fetal growth across gestation (18, 19, 34). Only fetuses that appeared morphologically normal were included for CRL measurement to examine intrauterine growth restriction (IUGR). There was no statistically significant difference in mean CRL in 10^3 PFU ZIKV-MEX or 10^3 PFU ZIKV-BRA fetuses compared to fetuses from PBS-inoculated controls at E11.5 (One-way ANOVA with Tukey's multiple comparisons, $p > 0.9797$) (**Figure 1D**). For 10^5 PFU ZIKV-MEX fetuses, there was not a statistically significant reduction in CRL at E14.5 (Tukey's multiple comparisons, $p = 0.2096$), which is consistent with 10^3 PFU ZIKV-MEX fetuses but different from 10^3 PFU ZIKV-BRA fetuses at E14.5 reported in reference (18). We observed a significant reduction in mean CRL in both 10^3 PFU ZIKV-BRA and 10^3 PFU ZIKV-MEX fetuses compared to PBS controls at E17.5 (One-way ANOVA with Tukey's multiple

157 comparisons, p <0.0001, average difference 3.24mm and 6.23mm, corresponding to an 11%
158 and 21% reduction in fetal size, respectively). Overall, these data indicate that 10^3 PFU ZIKV-
159 MEX and 10^3 PFU ZIKV-BRA both have the capacity to cause IUGR, but 10^3 PFU ZIKV-BRA-
160 induced IUGR manifests earlier in gestation and results in a greater magnitude of restriction.

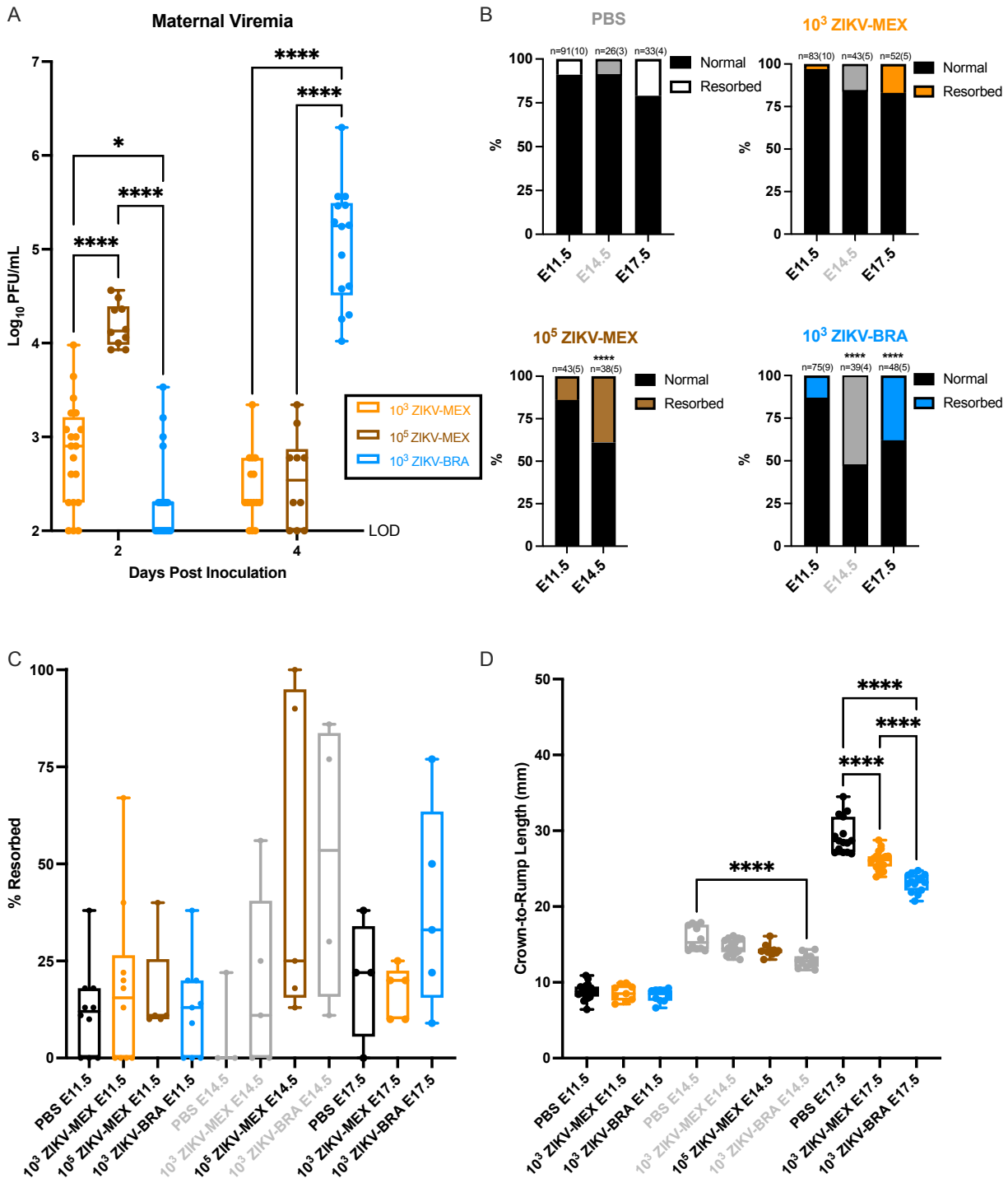

Figure 1: ZIKV strain phenotypic heterogeneity is present across gestation. (A) Time-mated *Ifnar1*$^{-/-}$ dams were inoculated with 10^3 PFU ZIKV-MEX, 10^5 PFU ZIKV-MEX, or 10^3 PFU ZIKV-BRA on E7.5. Maternal infection was assayed by plaque assay on 2, 4, and 7 days post inoculation, and significance was determined by one-way ANOVA. (B) Rate of normal (black) versus resorbed (colored) fetuses at E11.5, E14.5, and E17.5 after maternal infection at E7.5. Data are presented as the percent of n = 23-83 total fetuses (from 3 to 10 dams per treatment group). Significance was determined by Fisher's exact test. (C) Pregnancy outcomes of individual animals in each treatment group. Data are presented as percent of fetuses resorbed in each pregnancy. (D) Crown-to-rump length measurements in mm of morphologically normal fetuses at E11.5, E14.5, and E17.5 using ImageJ software.

Significance was determined by one-way ANOVA. The color gray indicates historical data from reference (18).
Significance annotations for all figures: ****, $P \leq 0.0001$; ***, $P \leq 0.001$; **, $P \leq 0.01$; *, $P \leq 0.05$.

To understand how or if infectious ZIKV virions reach the developing embryo during gestation, we examined a subset of MFI tissues for the presence of infectious virus using plaque assays. The MFI is composed of the maternal-derived decidua and the fetal-derived placenta. Consistent with our previous work (18), no infectious virus, except for one sample at E11.5, was detected by plaque assay in any fetus sample for any treatment group (**Figure 2A**). In contrast, infectious virus was detected in about one third of MFI samples from ZIKV-infected groups. At E11.5, 10^5 PFU ZIKV-MEX MFIs had a significantly higher titer than 10^3 PFU ZIKV-MEX MFIs (Tukey's multiple comparisons, p = 0.0028)(**Figure 2A**). However, at E14.5, 10^3 PFU ZIKV-BRA MFIs had a significantly higher titer than both ZIKV-MEX-inoculated groups (Tukey's multiple comparisons, p < 0.0001)(**Figure 2A**).

Given the limited evidence for viral replication in fetuses or at the MFI, we next used RT-qPCR to examine these tissues for the presence of ZIKV viral RNA (vRNA)—RT-qPCR detects viable, partial, and non-viable RNA fragments. The presence of vRNA has been shown to induce antiviral signaling and synthesis of viral proteins (35), and therefore can trigger an antiviral response. We first analyzed archived MFI and fetus samples at E14.5 from reference (18). We observed no difference in MFI vRNA load between any ZIKV-inoculated groups (2-way ANOVA with Tukey's multiple comparisons, p > 0.2470)(**Figure 2B**). We did, however, observe significantly higher fetal vRNA loads in 10^3 PFU ZIKV-BRA and 10^5 PFU ZIKV-MEX groups compared to 10^3 PFU ZIKV-MEX (Tukey's multiple comparison, p < 0.0022)(**Figure 2B**), suggesting that ZIKV-MEX vRNA can reach the fetus at the same rate as ZIKV-BRA vRNA at higher doses. Given these differences, we dissected the MFI into the maternal-derived decidua and the fetal-derived placenta at E11.5 to better understand the vRNA burden in distinct MFI structures before fetal resorption is clearly evident. At E11.5, we observed high vRNA loads in all ZIKV-inoculated groups. 10^3 PFU ZIKV-BRA had significantly higher vRNA loads in all

196 tissues compared to 10^3 PFU ZIKV-MEX ($p < 0.0001$), but not 10^5 PFU ZIKV-MEX at E11.5
197 (Tukey's multiple comparisons, $p = 0.6605$). These data demonstrate that vRNA load is
198 dependent on the dose and the genotype of the infecting ZIKV strain, with significant differences
199 in vRNA loads observed in the decidua, placenta, and fetus prior to (E11.5) and when (E14.5)
200 fetal resorption is detectable (**Figure 2B**).

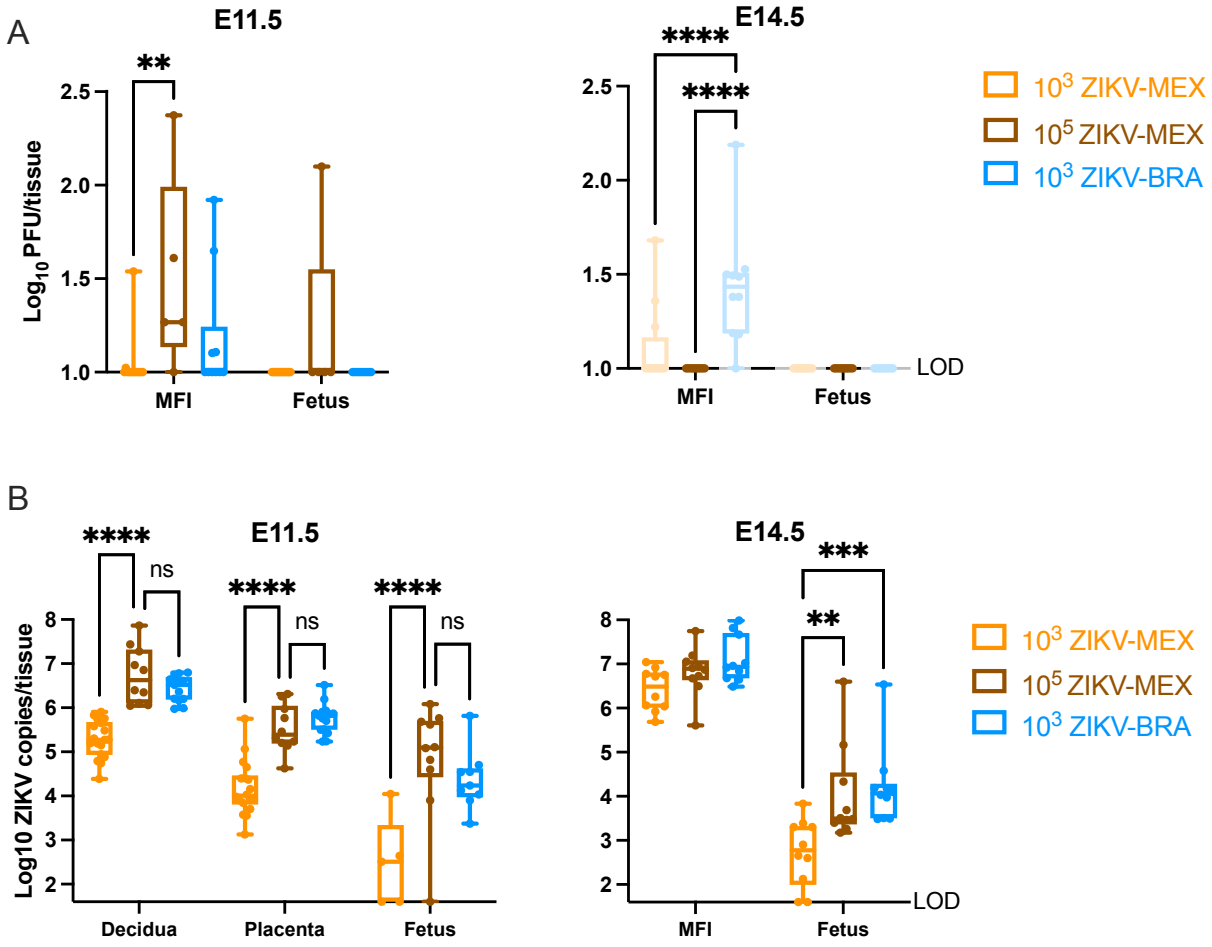

201

202 **Figure 2: Infectious virus and ZIKV vRNA load at E11.5 and E14.5.** (A) Tissue titer was measured by plaque
203 assay for homogenized MFI (comprising decidua and placental tissues) and fetuses at E11.5 and E14.5. (B) ZIKV
204 vRNA load was measured by qRT-PCR for homogenized decidua, placenta, MFI, and fetuses at E11.5 and E14.5.
205 For all figures, symbols represent individual MFI or fetus samples from 4 to 10 independent experiments for each
206 treatment group. The color gray indicates historical data from reference (Bohm 2021). Bars represent the median viral
207 titer of each treatment group and significance was determined by two-way ANOVA with Tukey's multiple
208 comparisons. Significance annotations: ****, $P \leq 0.0001$; ***, $P \leq 0.001$; **, $P \leq 0.01$; *, $P \leq 0.05$; ns, $P > 0.05$.

209

210

ZIKV influences the MFI transcriptome in a strain- and dose-dependent manner.

Phenotypic characterization across gestation established that infection with 10^3 PFU ZIKV-BRA and 10^5 PFU ZIKV-MEX results in significantly greater fetal demise and vRNA load in MFI tissues compared to infection with 10^3 PFU ZIKV-MEX. We therefore sought to determine how infiltration of ZIKV vRNA impacts the function of the MFI, with the aim of identifying potential mechanisms of fetal resorption. We collected deciduas and placentas from dams (n=5 per treatment group) that were inoculated with 10^3 PFU ZIKV-MEX, 10^5 PFU ZIKV-MEX, and 10^3 PFU ZIKV-BRA or PBS. Decidua and placenta tissue samples were collected at E9.5 and E11.5. These timepoints were chosen because fetal resorption can be a multi-day, four-stage process (36). We therefore aimed to capture early responses that may be important for driving the resorption process. Additionally, the MFI can be dissected into functionally distinct tissues (decidua and placenta) that are large enough to isolate total RNA from a single sample without pooling. We included equal proportions of male and female decidua and placenta tissues, with one or two tissues per embryo sex per animal to avoid sex biases in our dataset. These numbers also ensured robust sampling from each pregnancy, which is critical given the broad range in fetal resorption we observed at E14.5 (see **Figure 1C**). We used DESeq2(37) to identify significantly differentially expressed genes (≥ 1 $\log_2$ fold, $p < 0.05$), Hallmark Gene Set Enrichment Analysis (Hallmark GSEA)(38, 39) to identify enriched gene families, and Pathview (40) to map differentially expressed genes to KEGG signaling pathways.

At E9.5, only five transcripts were significantly differentially expressed between PBS, 10^3 PFU ZIKV-MEX, and 10^3 PFU ZIKV-BRA deciduas. In contrast, 52 transcripts were significantly differentially expressed in the placenta (**Figure 3A-C**). The majority of these transcripts were differentially expressed between ZIKV-infected and PBS groups (**Figure 3A-B**), and only four transcripts differentially expressed between 10^3 PFU ZIKV-MEX and 10^3 PFU ZIKV-BRA (**Figure 3C**)(**Table 2**). Hallmark GSEA revealed that 10^3 PFU ZIKV-MEX and 10^3 PFU ZIKV-

BRA E9.5 placentas were enriched for IFN alpha and gamma responses compared to PBS (**Figure 3D-E**). Hallmark gene sets are coherently expressed signatures derived by aggregating many Molecular Signature Database (MSigDB) mouse gene sets to represent well-defined biological states or processes (38, 39). The Hallmark "IFN alpha response" comprises type I and type III IFN responses. Hallmark GSEA revealed that 10^3 PFU ZIKV-BRA E9.5 placentas are enriched for IFN alpha and gamma responses compared to 10^3 PFU ZIKV-MEX (**Figure 3F**). Additional signatures enriched in 10^3 PFU ZIKV-BRA compared to 10^3 PFU ZIKV-MEX include IL-6 JAK STAT3 signaling and heme, bile acid, and xenobiotic metabolism. 10^3 PFU ZIKV-MEX was enriched for MYC targets V1 and G2M checkpoint (**Figure 3F**). At E9.5, there was no significant fetal resorption, nor infectious virus detected in the MFI across inoculated strains and doses (**Figure 3G-H**). There were no significant differences in ZIKV vRNA loads in the decidua, placenta, or fetus samples between 10^3 PFU ZIKV-MEX and 10^3 PFU ZIKV-BRA (Two-way ANOVA with Sidak's multiple comparisons, $p > 0.1445$)(**Figure 3I**).

Gene ID	Log_2 fold change (10^3 PFU ZIKV-BRA vs 10^3 PFU ZIKV-MEX)	adj p value	Predicted function
Ntn3	1.40	0.04	Animal organ morphogenesis; neuron projection development; and tissue development
Zfp654	1.67	0.03	DNA-binding transcription factor activity, RNA polymerase II-specific, expressed in early conceptus
Gm17711	2.15	0.05	Not annotated
Gm21742	2.62	0.05	Not annotated

Table 2: Differential gene expression between ZIKV-BRA and ZIKV-MEX in E9.5 placentas.

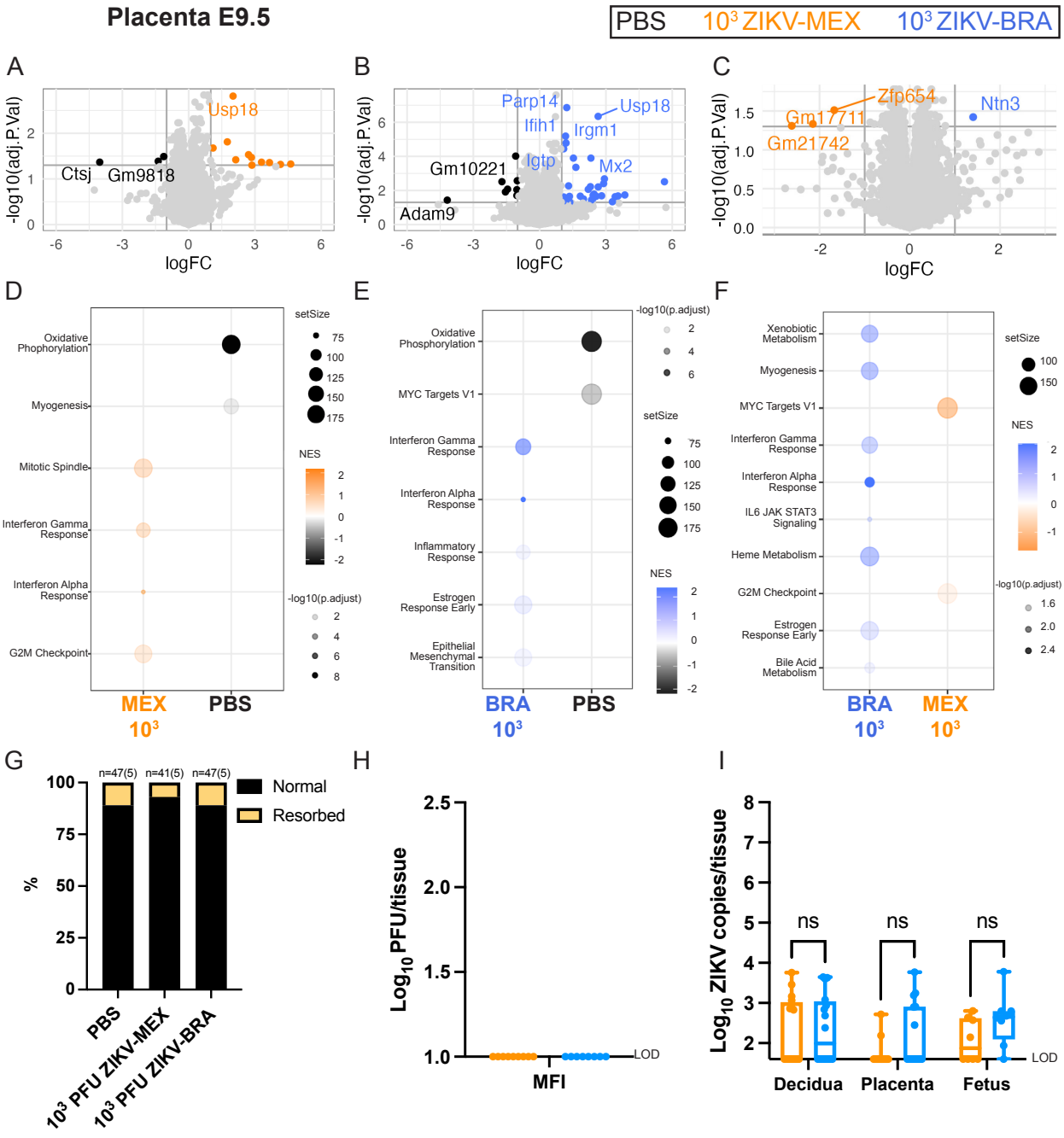

Figure 3: ZIKV-induced transcriptome differences in the E9.5 placenta. (A-C) Volcano plots depicting differentially expressed gene transcripts in the placenta at E9.5 of animals inoculated with 10^3 PFU ZIKV-MEX, 10^3 PFU ZIKV-BRA, or PBS. Genes with significant changes |log 2 fold change| >1 and -log10(p.adjust) > 0.05 appear in color; genes outside these parameters appear in light gray. (D-F) Hallmark gene set enrichment analysis of differentially expressed genes between ZIKV-infected and PBS groups. Transcriptomic data represent 16-20 embryo sex-balanced placentas from n=5 dams per inoculation group. PBS = black, 10^3 PFU ZIKV-MEX = orange, 10^3 PFU ZIKV-BRA = blue. (G) Rate of normal (black) versus resorbed (yellow) fetuses at E9.5 after maternal inoculation at E7.5. Data are presented as the percent of n = 41-47 total fetuses (from 5 dams per treatment group). (H) Tissue titer was measured by plaque assay for homogenized MFI (comprising decidua and placental tissues) at E9.5 for 8-9 replicates per treatment group. (I) ZIKV vRNA load in decidua, placenta, and fetuses at E9.5 was measured by qRT-PCR for 8-16 replicates per treatment group. Significance was determined by two-way ANOVA with Sidak's multiple comparisons. Significance annotations: ns, $P > 0.05$.

At E11.5, we identified 179 gene transcripts that were significantly differentially expressed in the decidua, with most occurring between ZIKV-infected and PBS groups (**Figure 4A-C**). Hallmark GSEA revealed that 10^3 PFU ZIKV-MEX, 10^5 PFU ZIKV-MEX, and 10^3 PFU ZIKV-BRA transcriptomes were enriched for the IFN alpha and gamma responses, as well as allograft rejection (**Figure 4D-F**). We identified multiple transcripts that were significantly differentially expressed between ZIKV-infected groups (**Figure 4G-I**). We identified transcripts that were differentially expressed based on inoculation dose (10^3 PFU vs 10^5 PFU)(**Figure 4G**), the inoculating ZIKV strain (ZIKV-MEX vs ZIKV-BRA)(**Figure 4H**), and between two inoculations that cause similar rates of fetal resorption (10^5 PFU ZIKV-MEX, and 10^3 PFU ZIKV-BRA)(**Figure 4I**). Hallmark GSEA showed that the E11.5 10^5 PFU ZIKV-MEX decidua was enriched for the IFN alpha and gamma responses compared to 10^3 PFU ZIKV-MEX, which was enriched for oxidative phosphorylation, G2M checkpoint, and E2F targets (**Figure 4J**). 10^3 PFU ZIKV-BRA was also enriched for the IFN responses compared to 10^3 PFU ZIKV-MEX (**Figure 4K**). However, when 10^5 PFU ZIKV-MEX and 10^3 PFU ZIKV-BRA were compared, 10^5 PFU ZIKV-MEX was only enriched for IFN gamma and myogenesis gene sets (**Figure 4L**), indicating that these groups had similar enrichment for the type I IFN response. These data suggest that inoculum boluses containing strains or doses (10^5 PFU ZIKV-MEX and 10^3 PFU ZIKV-BRA) that result in significant rates of fetal demise also induce robust type I IFN responses in the decidua at timepoints just prior to fetal resorption becoming visibly detectable.

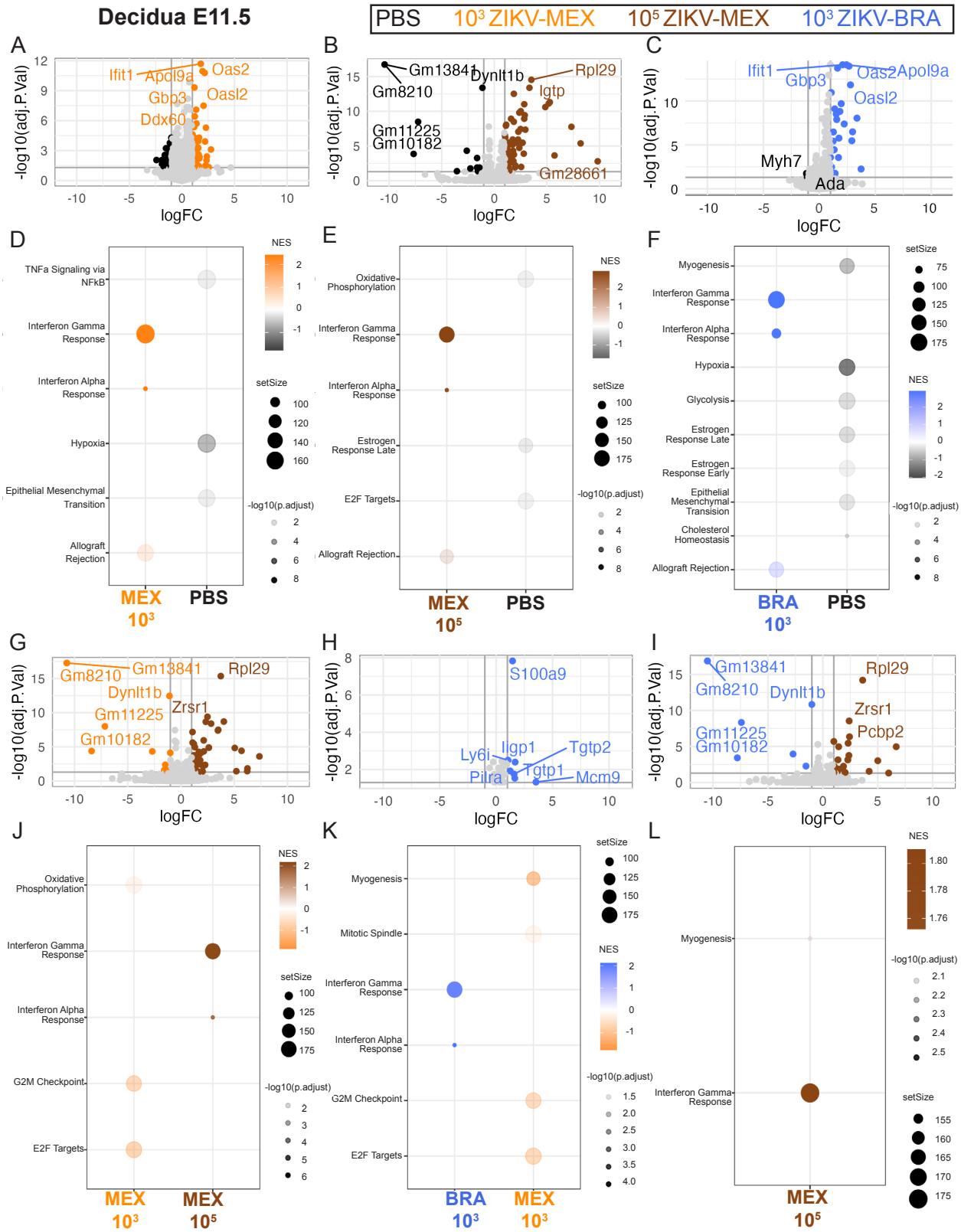

Figure 4: ZIKV strain and dose significantly influences the decidua transcriptome at E11.5. (A-C) Volcano plots depicting differentially expressed gene transcripts in the decidua at E11.5 of animals inoculated with 10^3 PFU ZIKV-MEX, 10^5 PFU ZIKV-MEX, or 10^3 PFU ZIKV-BRA and PBS. Genes with significant changes |log 2 fold change| >1

and -log10(p.adjust) > 0.05 appear in color; genes outside these parameters appear in light gray. (D-F) Hallmark gene set enrichment analysis of differentially expressed genes between ZIKV-infected and PBS groups. (G-I) Volcano plots depicting differentially expressed gene transcripts between ZIKV-infected animals in the decidua at E11.5. Genes with significant changes |log 2 fold change| >1 and -log10(p.adjust) > 0.05 appear in color; genes outside these parameters appear in lightgray. (J-L) Hallmark gene set enrichment analysis of differentially expressed genes between ZIKV-infected E11.5 deciduas. In all figures, 10^3 PFU ZIKV-MEX, 10^3 PFU ZIKV-BRA, PBS data represent 14-20 embryo sex-balanced deciduas from n=4-5 dams per inoculation group. 10^5 PFU ZIKV-MEX data represent three embryo sex-balanced deciduas from n=3 dams. PBS = black, 10^3 PFU ZIKV-MEX = orange, 10^5 PFU ZIKV-MEX = brown, 10^3 PFU ZIKV-BRA = blue.

In the placenta, we identified 540 gene transcripts that were significantly differentially expressed at E11.5. Most of these differences occurred between ZIKV-infected and PBS groups (**Figure 5A-C**). Similar to our observations in the decidua, 10^3 PFU ZIKV-MEX, 10^5 PFU ZIKV-MEX, and 10^3 PFU ZIKV-BRA E11.5 placentas were enriched for IFN responses and allograft rejection compared to PBS (**Figure 5D-F**). However, we also observed enrichment for the inflammatory response and MYC targets V1, suggesting that the placenta is subjected to more robust antiviral responses than the decidua.

We identified multiple transcripts from E11.5 placental tissue that were significantly differentially expressed among ZIKV-infected groups (**Figure 5G-I**). We identified transcripts that were differentially expressed based on inoculation dose (10^3 PFU vs 10^5 PFU)(**Figure 5G**), the inoculating ZIKV strain (ZIKV-MEX vs ZIKV-BRA)(**Figure 5H**), and between two inoculations that cause similar rates of fetal resorption (10^5 PFU ZIKV-MEX, and 10^3 PFU ZIKV-BRA)(**Figure 5I**). Hallmark GSEA revealed that the 10^5 PFU ZIKV-MEX and 10^3 PFU ZIKV-BRA placentas were enriched for the IFN alpha and gamma responses, inflammatory response, and TNFa signaling via NFkB compared to 10^3 PFU ZIKV-MEX (**Figure 5J-K**). However, when 10^5 PFU ZIKV-MEX and 10^3 PFU ZIKV-BRA were compared, 10^5 PFU ZIKV-MEX was enriched for the inflammatory gene set, but not TNFa signaling via NFkB nor the IFN alpha and gamma responses (**Figure 5L**), suggesting that 10^5 PFU ZIKV-MEX and 10^3 PFU ZIKV-BRA similarly induce these responses. Further, the enrichment scores (NES), number of genes enriched within a gene set (setSize), and adjusted p-values (-log10(p.adjust)) suggest that the IFN alpha and gamma responses are more robust than TNFa signaling via NFkB.

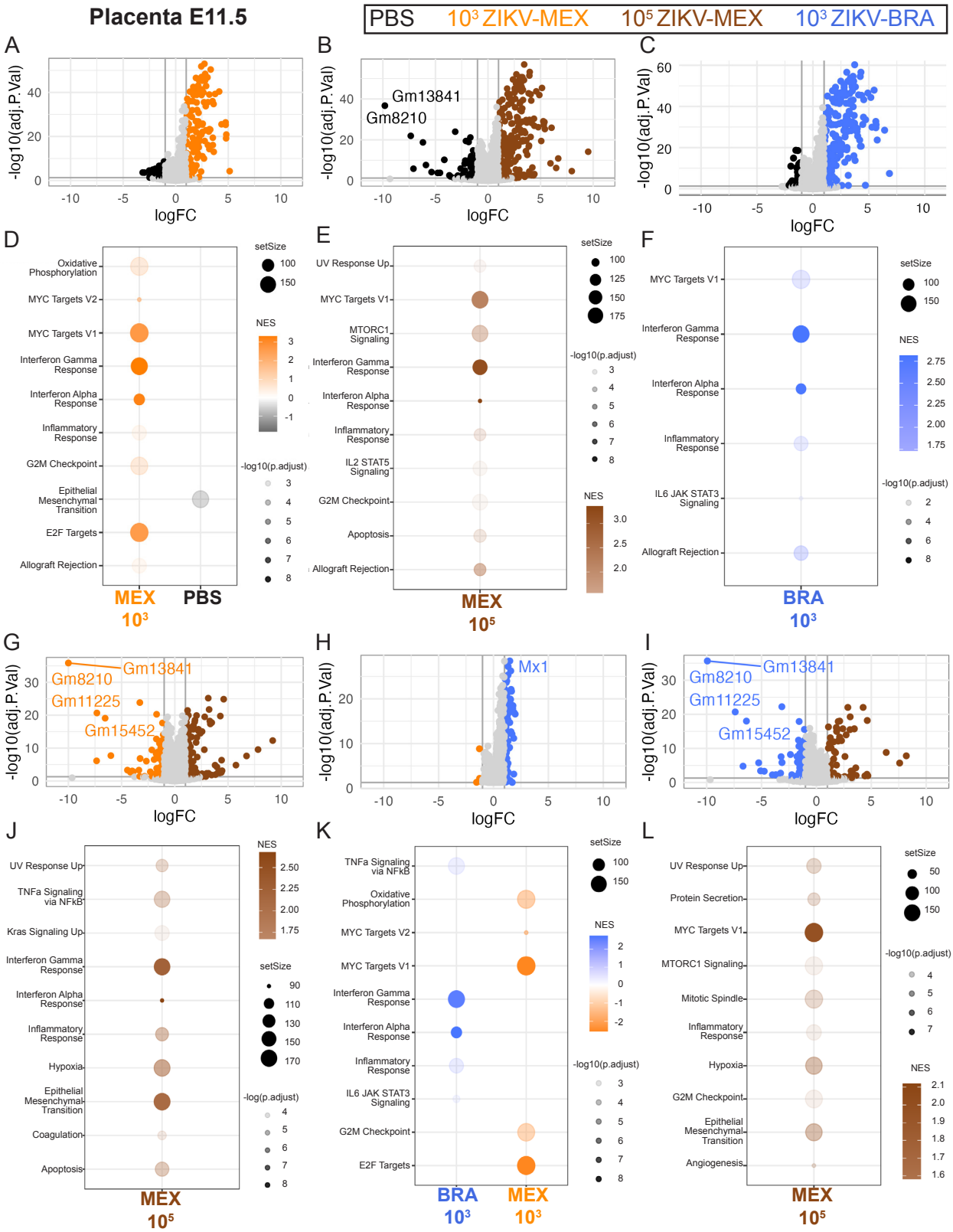

Figure 5: ZIKV strain and dose significantly influence the placenta transcriptome at E11.5. (A-C) Volcano plots depicting differentially expressed gene transcripts in the placenta at E11.5 of animals inoculated with 10^3 PFU ZIKV-MEX, 10^5 PFU ZIKV-MEX, or 10^3 PFU ZIKV-BRA and PBS. Genes with significant changes |log 2 fold change| >1

and -log10(p.adjust) > 0.05 appear in color; genes outside these parameters appear in lightgray. (D-F) Hallmark gene set enrichment analysis of differentially expressed genes between ZIKV-infected and PBS groups. (G-I) Volcano plots depicting differentially expressed gene transcripts between ZIKV-infected animals in the placenta at E11.5. Genes with significant changes |log 2 fold change| >1 and -log10(p.adjust) > 0.05 appear in color; genes outside these parameters appear in lightgray. (J-L) Hallmark gene set enrichment analysis of differentially expressed genes between ZIKV-infected E11.5 placentas. In all figures, data represent 12-20 embryo sex-balanced placentas from n=4-5 dams per inoculation group. PBS = black, 10^3 PFU ZIKV-MEX = orange, 10^5 PFU ZIKV-MEX = brown, 10^3 PFU ZIKV-BRA = blue.

We mapped the placenta transcriptome at E11.5 of 10^3 PFU ZIKV-MEX, 10^5 PFU ZIKV-MEX, and 10^3 PFU ZIKV-BRA (compared to PBS), to KEGG pathways using Pathview to identify homologous pathways that could be implicated in initiating the IFN response (**Figure 6**)(40). 10^5 PFU ZIKV-MEX and 10^3 PFU ZIKV-BRA had significant, uniform upregulation of genes in the TLR pathways, notably TLR3, which senses dsRNA (**Figure 6A-B**). When we compared 10^5 PFU ZIKV-MEX and 10^3 PFU ZIKV-BRA directly (**Figure 6C**), we observed variable expression of genes in TLR pathways, suggesting that these pathways were not uniformly expressed in animals that received ZIKV boluses that cause significant fetal resorption.

When we mapped 10^5 PFU ZIKV-MEX and 10^3 PFU ZIKV-BRA to the RIG-I-like receptor (RLR) pathway, we observed significant, uniform upregulation of genes compared to 10^3 PFU ZIKV-MEX (**Figure 7A-B**). In contrast to our findings with the TLR pathway, we observed almost no significant differential expression of genes in the RLR pathway between 10^5 PFU ZIKV-MEX and 10^3 PFU ZIKV-BRA (**Figure 7C**), suggesting that 10^5 PFU ZIKV-MEX and 10^3 PFU ZIKV-BRA uniformly induce RLR signaling compared to 10^3 PFU ZIKV-MEX.

Next, we aimed to understand the association between ZIKV vRNA and the RLR-driven IFN response. ZIKV infection produces single- and double-stranded RNA intermediates during viral replication that can signal through RLRs and toll-like receptors (TLRs), which operate to induce antiviral factors including IFN and proinflammatory cytokines. We therefore plotted gene expression of IFN-response genes (*Rsad2*, *Mx1*, and *Stat2*), ZIKV pattern-recognition receptors (*Ddx58* aka RIG-I, *Ifih1* aka MDA5, and *Tlr3*), a proinflammatory cytokine (*Il1a*), and *Actin* (as a control)(**Figure 8**). We found that IFN-response genes were significantly, and proportionally

355 expressed when compared to the vRNA load ($p < 0.0001$)(**Figure 8A-C**). RLR genes *Ddx58*
356 and *Ifih1* were also significantly proportionally expressed ($p < 0.0005$) while *Tlr3* was not ($p =$
357 0.211), suggesting that ZIKV infection preferentially induces RLR expression over other pattern-
358 recognition receptors (**Figure 8D-F**). These results are consistent with those from our Pathview
359 analysis, demonstrating that RLR pathways are uniformly upregulated by the two infectious
360 boluses that result in high vRNA loads at the MFI and cause significant fetal resorption, while
361 TLRs are not. The gene *Il1a* was not significantly proportionally expressed ($p = 0.238$) in
362 relation to vRNA load suggesting that genes involved in proinflammatory cytokine production
363 are not proportional to ZIKV vRNA (**Figure 8G**).

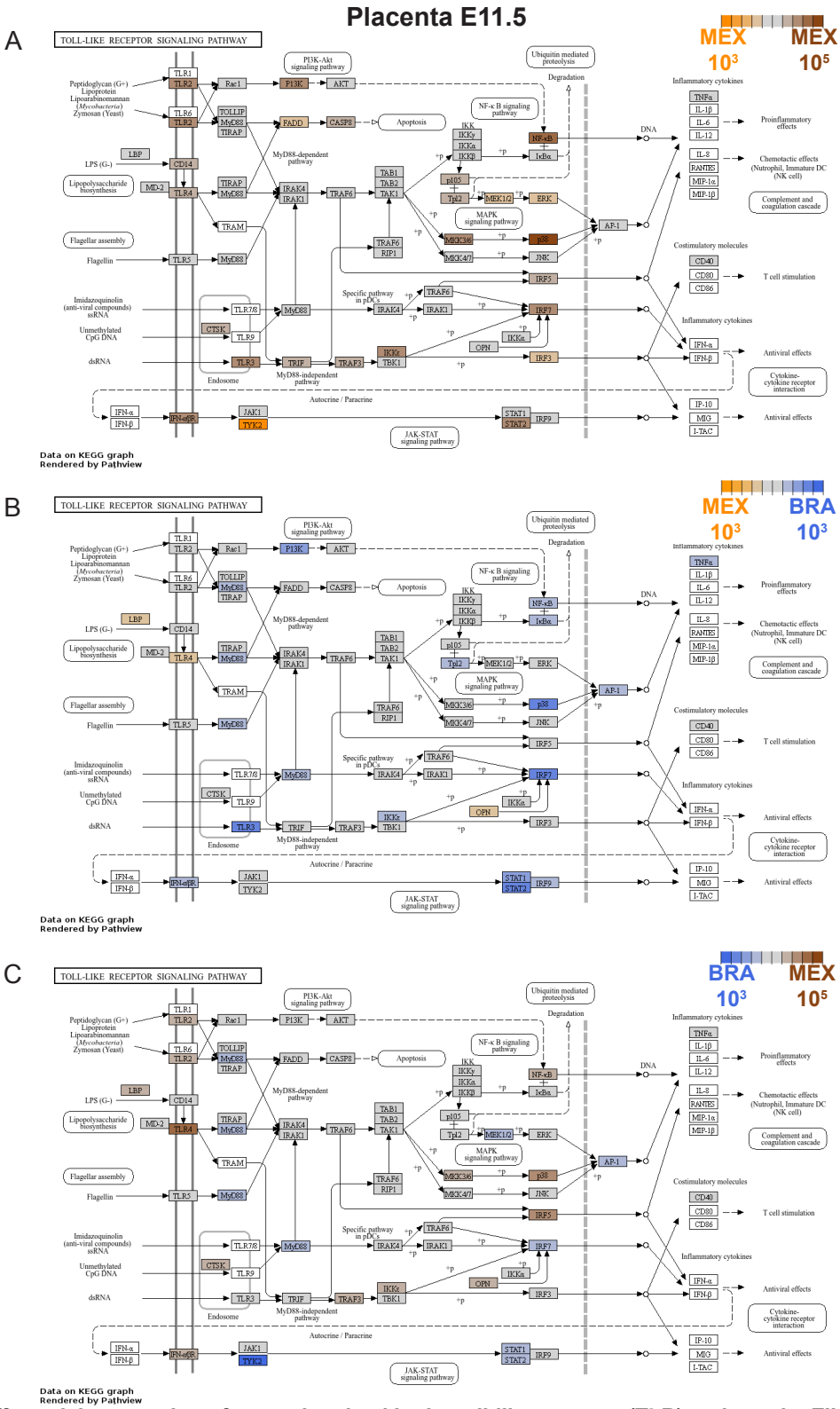

Figure 6: Differential expression of genes involved in the toll-like receptor (TLR) pathway by ZIKV-infected animals in the E11.5 placenta. (A-C) Genes with significant differential expression (-log10(p.adjust) > 0.05) in the E11.5 placenta were mapped to the TLR pathway using Pathview: 10^3 PFU ZIKV-MEX = orange, 10^5 PFU ZIKV-MEX = brown, 10^3 PFU ZIKV-BRA = blue. Genes that were not significantly differentially expressed appear in gray. Genes not analyzed appear in white. In all figures, data represent 12-20 embryo sex-balanced placentas from n=4-5 dams per inoculation group.

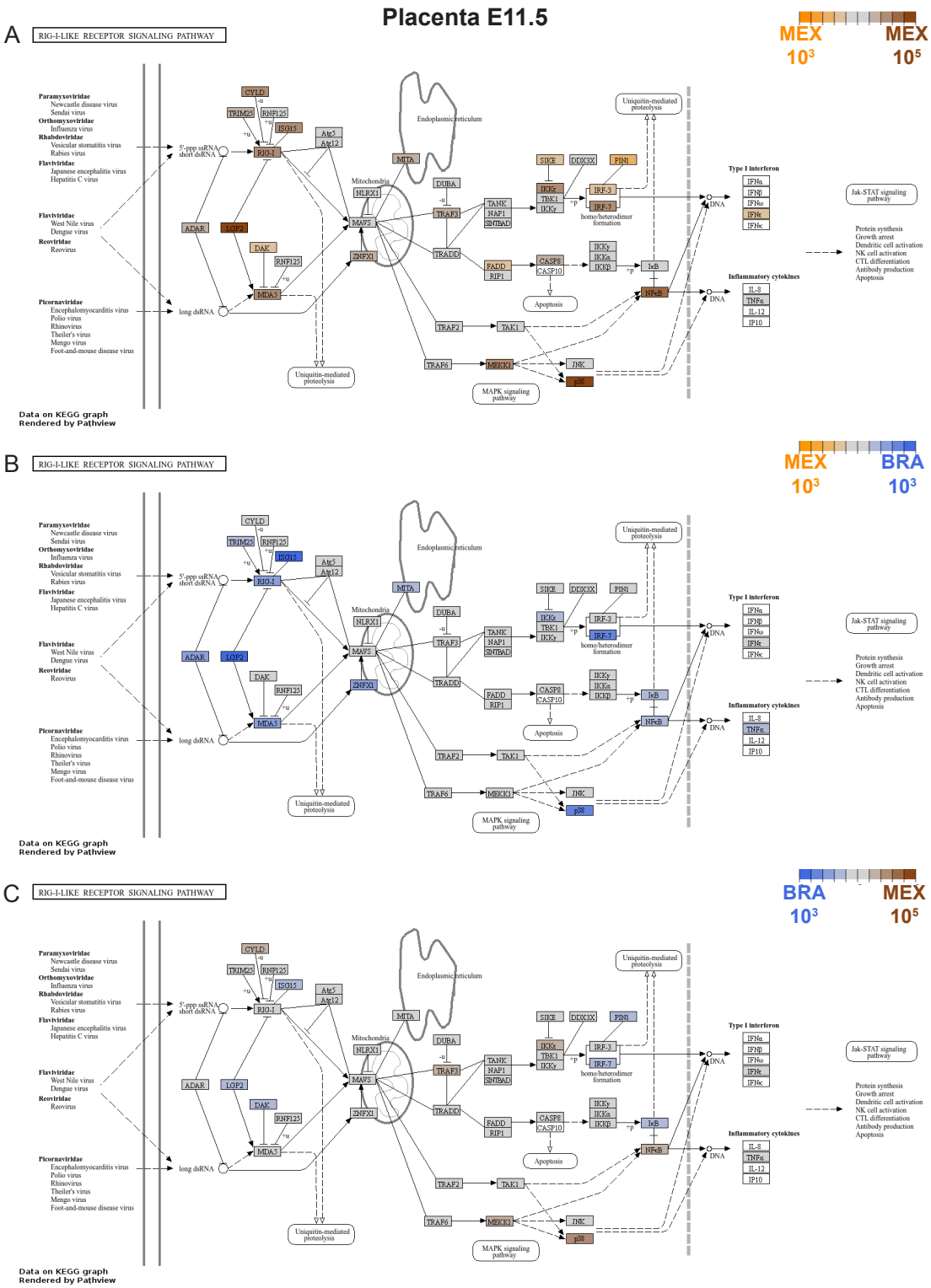

Figure 7: 10^5 PFU ZIKV-MEX and 10^3 PFU ZIKV-BRA uniformly induce expression of genes in the RIG-I-like receptor (RLR) pathway in the E11.5 placenta. (A-C) Genes with significant differential expression (-log10(p.adjust) > 0.05) in the E11.5 placenta were mapped to the RLR pathway using Pathview: 10^3 PFU ZIKV-MEX = orange, 10^5 PFU ZIKV-MEX = brown, 10^3 PFU ZIKV-BRA = blue. Genes that were not significantly differentially expressed appear in gray. Genes not analyzed appear in white. In all figures, data represent 12-20 embryo sex-balanced placentas from n=4-5 dams per inoculation group.

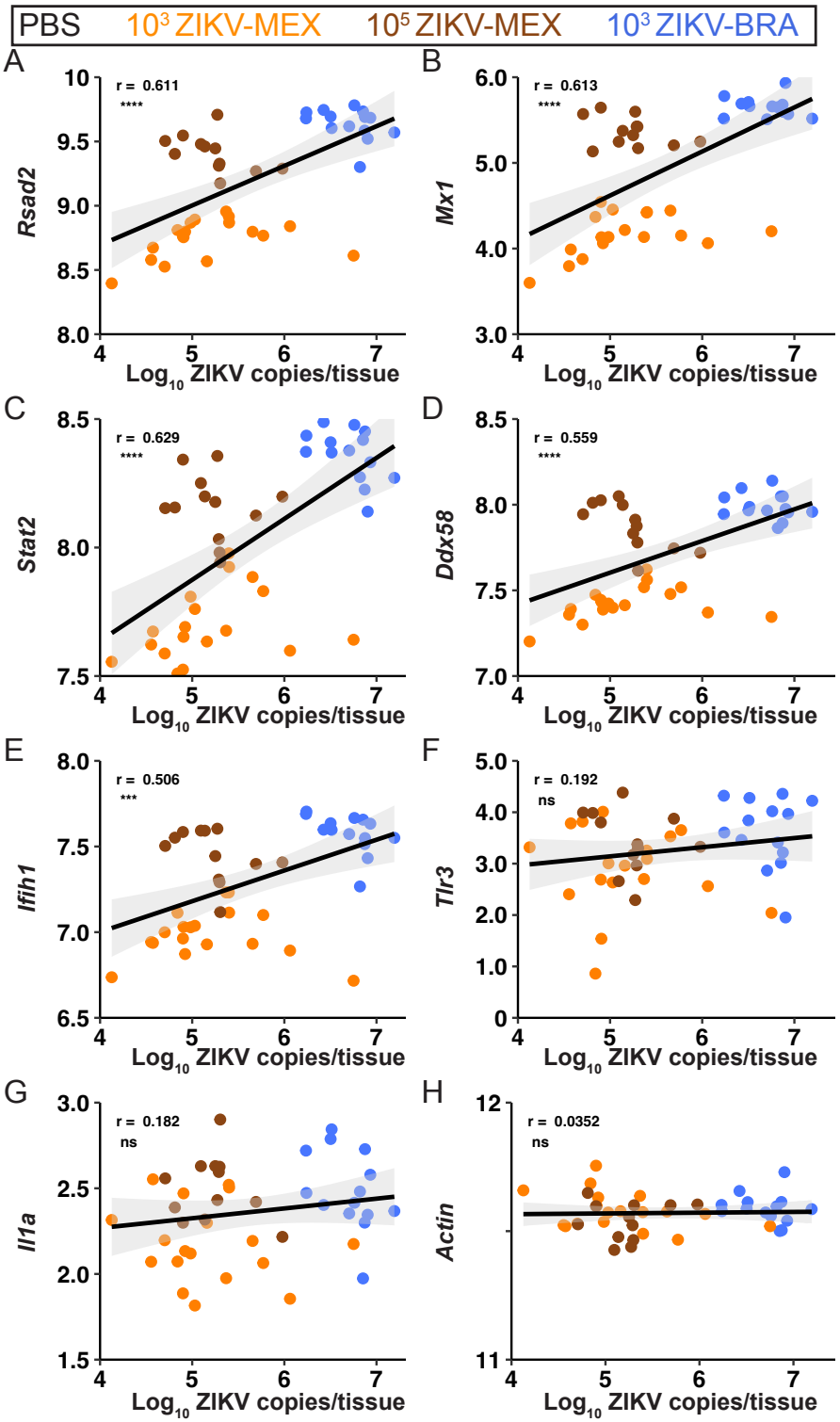

Figure 8: ZIKV vRNA load positively correlates with interferon-stimulated genes and RLRs. Pearson correlations with 95% confidence intervals are shown for ZIKV vRNA copies/tissue versus transcript counts (in counts per million reads) for interferon-stimulated genes *Rsad2*, *Mx1*, *Stat2* (A-C), RLR genes *Ddx58* and *Ifih1* (D-E), *Tlr3* (F), proinflammatory cytokine *Il1ra* (G), and *Actin* (H). Symbols represent individual placentas from 4-5 dams inoculated with 10^3 PFU ZIKV-MEX (orange), 10^5 PFU ZIKV-MEX (brown), or 10^3 PFU ZIKV-BRA (blue). Correlation coefficients (r) are shown in each panel. Significance annotations for all figures: ****, $P \leq 0.0001$; ***, $P \leq 0.001$; **, $P \leq 0.01$; *, $P \leq 0.05$; ns, > 0.05.

383 **Modest chemical inhibition of RIG-I activity in the placenta does not reduce the likelihood**
384 **of fetal demise during ZIKV infection.**

385 The previous analyses suggested that ZIKV vRNA induces a proportional IFN response via
386 RLRs at the MFI that can instigate fetal demise. We therefore hypothesized that vRNA sensing
387 via RIG-I is contributing to fetal demise, because RIG-I has previously been shown to be the
388 primary sensor of ZIKV vRNA (41, 42). To investigate this, we used RIG012, a potent chemical
389 inhibitor of RIG-I, to reduce RIG-I activity in pregnant *Ifnar1*$^{-/-}$ mice (**Figure 9A**). RIG012 is
390 transient in serum, but stable in tissue (**Figure 9B-C**). We therefore aimed to maximize RIG012
391 concentration at the MFI over the course of our experiment. We intraperitoneally injected
392 22.5mg/kg RIG012 every 12 hours from E6.5 - E14.5, which resulted in significant tissue
393 permanence, averaging 0.65μM at the MFI (**Table 3**)(**Figure 9C**). This dose was well-tolerated
394 with no signs of toxicity. A concentration of 0.65μM RIG012 is estimated to reduce RIG-I activity
395 by ~40% according to *in vitro* data (43). We could not dose animals with concentrations higher
396 than this because 45mg/kg RIG012 caused lethal toxicity within 36 hours.
397

Group (number of animals)	**Inoculation at E7.5**	**Treatment**
Vehicle/PBS (n=10)	PBS	Vehicle: 15uL/g DMSO/Tween80/PBS every 12 hours E6.5 - E14
RIG012/PBS (n=7)	PBS	22.5mg/kg RIG012 every 12 hours E6.5 - E14
Vehicle/ZIKV-BRA (n=11)	10^3 PFU ZIKV-BRA	Vehicle: 15uL/g DMSO/Tween80/PBS every 12 hours E6.5 - E14
Vehicle/ZIKV-BRA (n=10)	10^3 PFU ZIKV-BRA	22.5mg/kg RIG012 every 12 hours E6.5 - E14

398 **Table 3**: RIG012 Treatment and ZIKV-BRA infection of pregnant Ifnar1$^{-/-}$ mice.

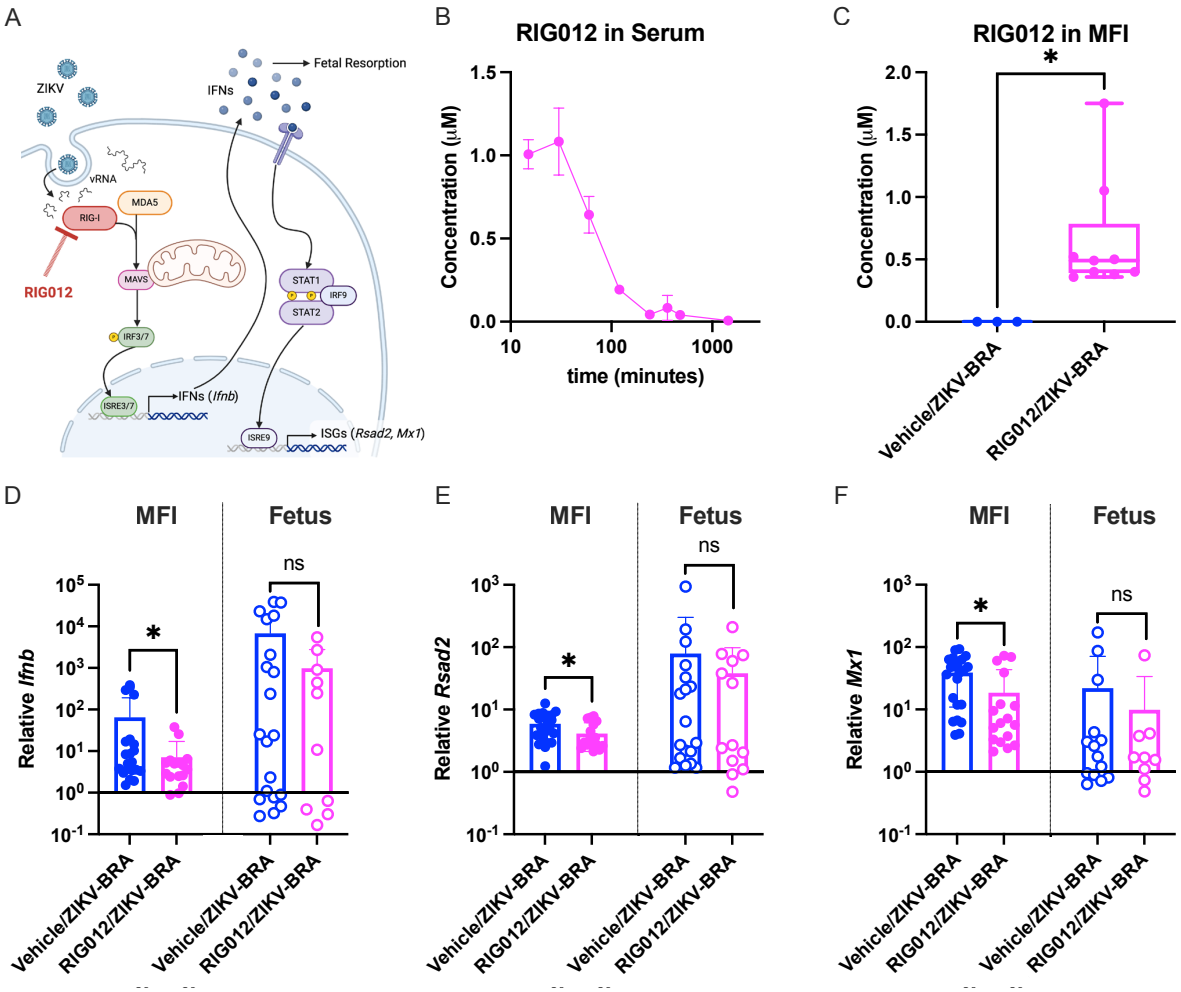

Figure 9: RIG012 treatment significantly inhibits RIG-I activity in the MFI. (A) Schematic of where RIG012 inhibits activity in the RLR-signaling pathway and downstream interferon (IFN) and interferon-stimulated genes (ISGs) that are expressed. (B) Concentration of RIG012 in serum of nonpregnant female mice (n=3) intraperitoneally injected once with 10mg/kg, measured by mass spectrometer. The mean with standard deviation is plotted. (C) Concentration of RIG012 in MFI at E14.5 of 10^3 PFU ZIKV-BRA-infected animals, intraperitoneally injected every 12 hours with Vehicle or 22.5mg/kg RIG012 E6.5-E14. Whole tissue samples were homogenized in water and concentration was measured via mass spectrometer. Bars represent the median concentration and significance was determined using an unpaired t-test. Transcript abundance of *Ifnb* (D), *Rsad2* (E), and *Mx1* (F) was analyzed from MFI and fetus samples collected on E14.5 by qPCR. Expression levels were normalized to *Hprt* and the ddC_T was calculated relative to samples harvested from PBS-inoculated controls. Data points represent individual samples. The mean with standard deviation is plotted. Significance was calculated with a t-test with Welch's correction. Significance annotations for all figures: ****, $P \leq 0.0001$; ***, $P \leq 0.001$; **, $P \leq 0.01$; *, $P \leq 0.05$; ns, > 0.05.

To assess whether our RIG012 treatment schedule was sufficient to interfere with RIG-I activation *in vivo* we measured relative transcript abundance of *Ifnb*, *Rsad2*, and *Mx1* in the MFI because these genes are known indicators of RIG-I activity (43). At E14.5, the MFI of animals treated with RIG012 and challenged with 10^3 PFU ZIKV-BRA (Vehicle/ZIKV-BRA) had significantly lower *Ifnb*, *Rsad2*, and *Mx1* expression than animals mock-treated with vehicle and

challenged with 10^3 PFU ZIKV-BRA (RIG012/ZIKV-BRA) ($p = 0.049$, 0.026, and 0.022, respectively)(**Figure 9D-F**). Fetuses from Vehicle/ZIKV-BRA and RIG012/ZIKV-BRA groups had no difference in relative *Ifnb*, *Rsad2*, and *Mx1* expression ($p = 0.057$, $p = 0.463$, and $p = 0.437$, respectively).

To evaluate the extent to which RIG012 treatment protects against ZIKV-induced fetal demise, we subcutaneously inoculated RIG012-treated and vehicle-treated pregnant *Ifnar1*$^{-/-}$ mice in the footpad with 1×10^3 PFU ZIKV-BRA, or phosphate buffered saline (PBS) to serve as experimental controls. The proportion of resorbed fetuses for RIG012/PBS did not differ significantly from Vehicle/PBS (16% vs. 11%; Fisher's exact test, $p = 0.4083$)(**Figure 10A**). Consistent to what we have reported previously (18), Vehicle/ZIKV-BRA induced a rate of resorption that was significantly higher than Vehicle/PBS group (43% vs. 11%; Fisher's exact test, $p < 0.0001$)(**Figure 10A**). However, no differences were observed in the proportion of resorbed fetuses in RIG012/ZIKV-BRA groups compared to Vehicle/ZIKV-BRA groups (41% vs 43%; Fisher's exact test, $p = 0.8861$)(**Figure 10A**), demonstrating that at this dose, RIG012 treatment did not protect from ZIKV-induced fetal demise.

We collected serum at 2, 4, and 7 dpi to compare viremia kinetics between Vehicle- and RIG012-treated animals. There were no significant differences in serum titers between Vehicle/ZIKV-BRA and RIG012/ZIKV-BRA at any time point (Two-way ANOVA, $p > 0.9999$) (**Figure 10B**). At E14.5 we collected MFI and fetal tissues; we used plaque assay to quantify infectious virus present and qRT-PCR to determine ZIKV vRNA loads. We found no significant difference in infectious virus at the MFI, and fetuses had undetectable levels of infectious virus (Two-way ANOVA with Sidak's multiple comparisons, $p > 0.9990$)(**Figure 10C**). There was no significant difference in ZIKV vRNA load of the MFI and fetus between RIG012- and Vehicle-treated animals (t-test with Welch's correction, $p = 0.3218$ and $p = 0.5515$, respectively)(**Figure 10D**).

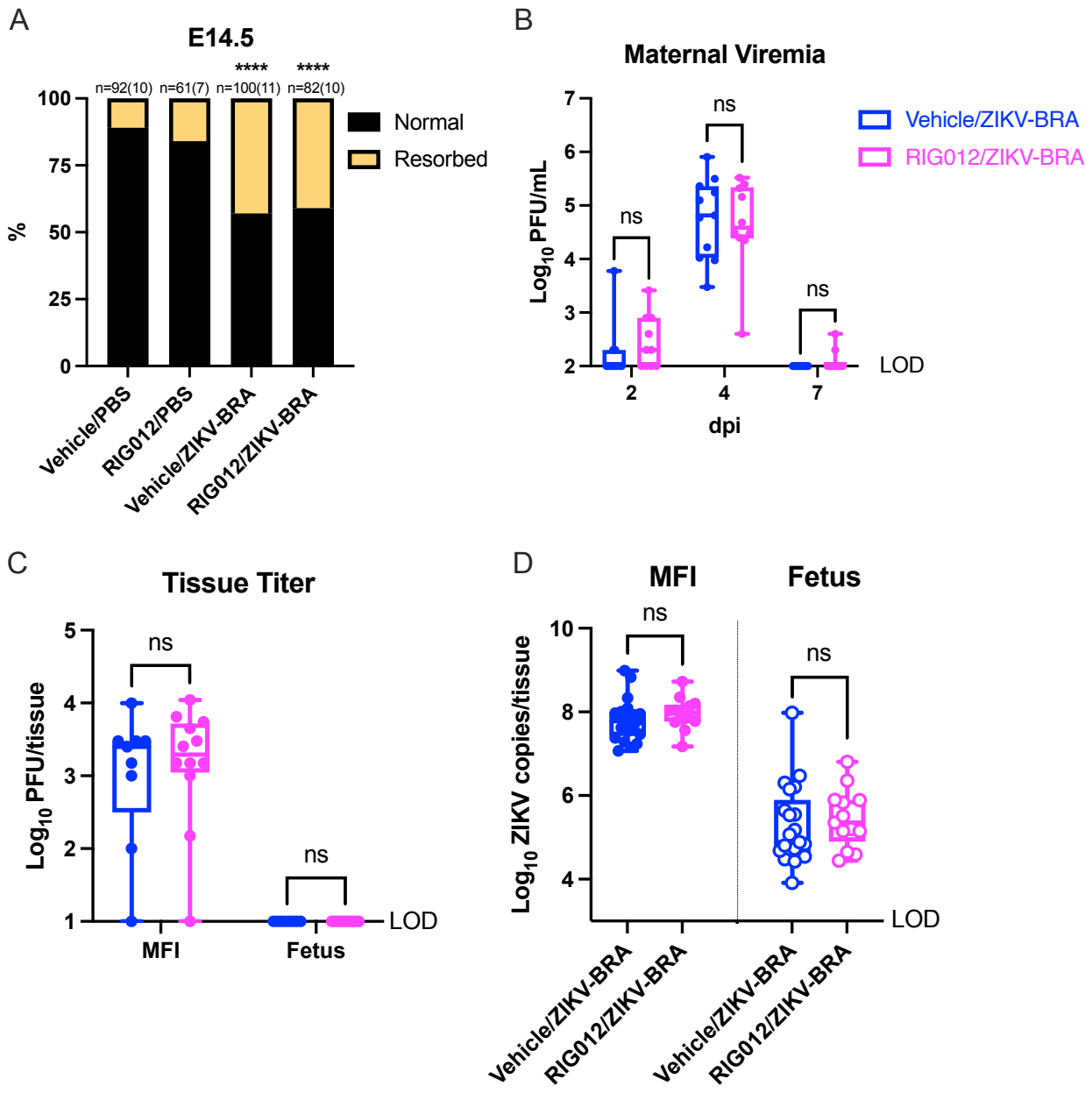

Figure 10: RIG012 treatment does not protect against fetal demise. (A) Time-mated *Ifnar1*$^{-/-}$ dams were treated with Vehicle or 22.5mg/kg RIG012 every 12 hours from E6.5-E14, inoculated with 10^3 PFU ZIKV-BRA on E7.5, and the rate of resorption was calculated at E14.5. Data are presented as the percent of n = 61-100 total fetuses (from 7 to 10 dams per treatment group). Significance was determined by Fisher's exact test. (B) Maternal viremia was assessed via plaque assay at 2, 4, and 7 days post inoculation (dpi) and significance was determined by two-way ANOVA with Tukey's multiple comparisons. (C) Tissue titer was assessed via plaque assay of MFI and fetus samples harvested at E14.5 and significance was determined by two-way ANOVA with Sidak's multiple comparisons (D) ZIKV vRNA load was assessed via qRT-PCR of MFI and fetus samples harvested at E14.5. Significance was determined by unpaired t-test. For all figures: ****, $P \leq 0.0001$; ***, $P \leq 0.001$; **, $P \leq 0.01$; *, $P \leq 0.05$; ns, > 0.05.

To evaluate whether there were differences in the MFI vRNA load or IFN response based on fetal outcome, we compared the vRNA load and relative transcript abundance of *Ifnb*, *Rsad2*, and *Mx1* between normal and resorbed concepti ("Outcome") among Vehicle/ZIKV-BRA and RIG012/ZIKV-BRA ("Treatment") groups (**Figure 11A-D**). Unexpectedly, the vRNA load of the MFI did not significantly differ between normal and resorbed Outcomes (Two-way ANOVA with Tukey's multiple comparisons, $p = 0.106$). None of the genes we compared were significantly differentially expressed in response to an interaction between Treatment and Outcome (Two-way ANOVA with Tukey's multiple comparisons, $p > 0.241$). Fetal Outcome was not significantly associated with MFI expression of *Ifnb*, *Rsad2*, and *Mx1* (Two-way ANOVA with Tukey's multiple comparisons, $p > 0.291$)(**Figure 11A-D**).

In contrast, we observed a significant association between fetal Outcome, fetal vRNA load, and fetal relative *Ifnb*, *Rsad2*, and *Mx1* expression (Two-way ANOVA with Tukey's multiple comparisons. $p < 0.041$)(**Figure 11A-D**). Resorbed fetuses had, on average, 1 $\log_{10}$ ZIKV copies/tissue more than normal fetuses (Two-way ANOVA with Tukey's multiple comparisons, $p = 0.002$). Resorbed fetuses also had nearly 10^4 higher relative *Ifnb* abundance (Two-way ANOVA with Tukey's multiple comparisons, $p = 0.019$), 10^2 higher relative *Rsad2* abundance (Two-way ANOVA with Tukey's multiple comparisons, $p = 0.041$), and $10^{1.7}$ higher relative *Mx1* abundance (Two-way ANOVA with Tukey's multiple comparisons, $p = 0.005$), compared to normal fetuses. Overall, resorbed fetuses had higher vRNA loads and IFN-stimulated gene expression than their normal counterparts.

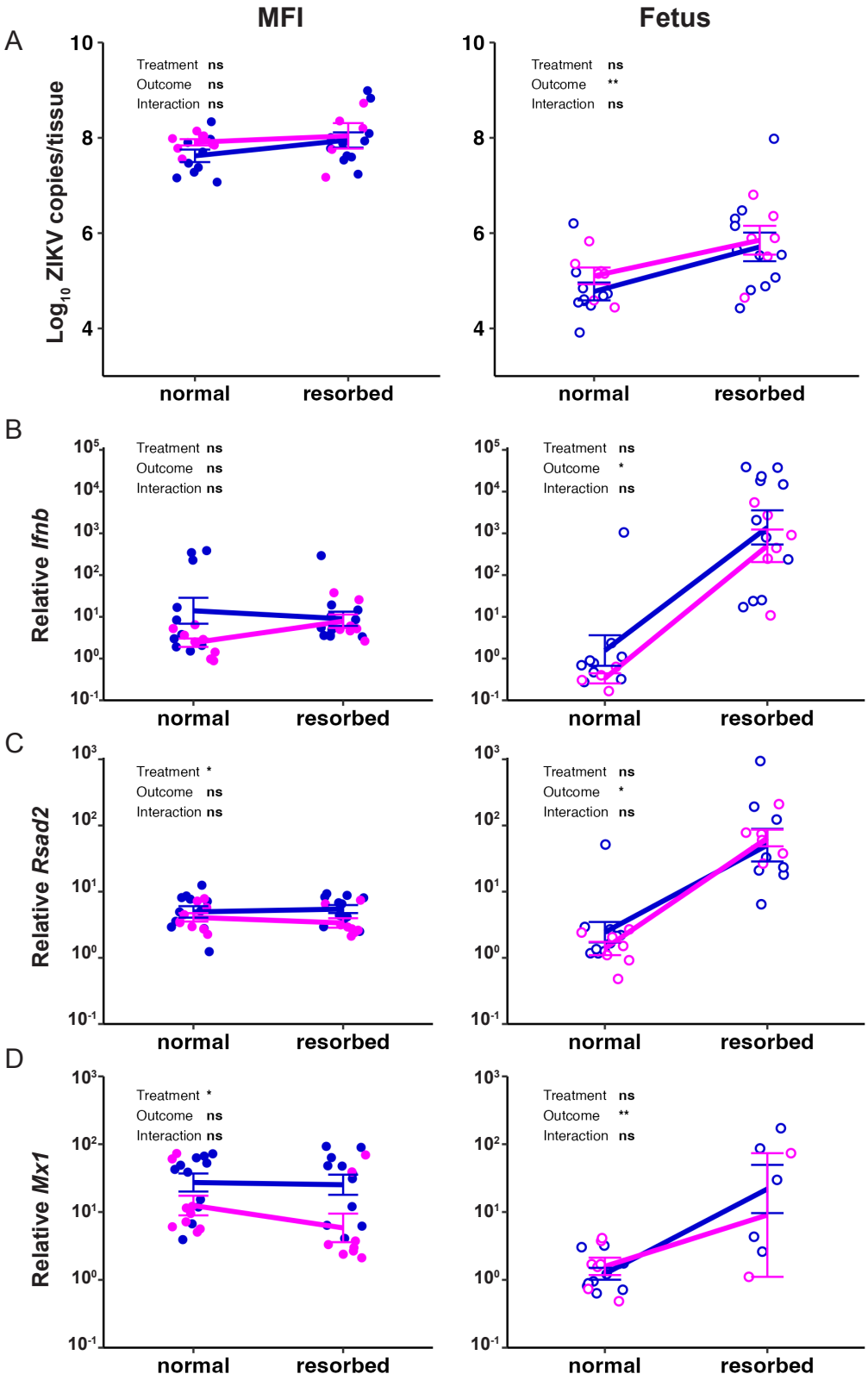

Figure 11: Resorbed fetuses have significantly higher relative interferon-stimulated gene expression than their normal counterparts. ZIKV vRNA load (A), relative *Ifnb* (B), *Rsad2* (C), and *Mx1* (D) expression in the MFI and fetus were plotted against Outcome (resorbed vs normal fetal outcome), and separated by Treatment (Vehicle vs 22.5mg/kg RIG012). Two-way ANOVA with Tukey's multiple comparisons was used to determine significance. For all figures: ****, $P \leq 0.0001$; ***, $P \leq 0.001$; **, $P \leq 0.01$; *, $P \leq 0.05$; ns, > 0.05.

DISCUSSION

Here, we expanded on our previous work (18), to demonstrate that ZIKV strain-dependent phenotypic heterogeneity is driven by antiviral immune signaling at the MFI and/or fetus. These observations substantially contribute to our nascent understanding of the mechanisms by which ZIKV harms the developing fetus. Our finding, that ZIKV activates a robust IFN response in the MFI prior to fetal resorption, is consistent with observations from other studies that mostly support a role for hyperinflammatory and/or hyperimmune responses as mediators of adverse fetal outcomes during congenital viral infections (17, 21, 44–47). For example, experiments using a breeding scheme that enabled the examination of pregnant dams that carry a mixture of fetuses that express type I IFN signaling (*Ifnar1*$^{+/-}$) or do not express type I IFN signaling (*Ifnar1*$^{-/-}$) within the same uterus found that only *Ifnar1*$^{+/-}$ fetuses were resorbed after ZIKV infection during early pregnancy, whereas their *Ifnar1*$^{-/-}$ littermates continued to develop (17). Similarly, experiments using mice lacking the IFN lambda (IFN-λ) receptor found that IFN-λ can have either a protective antiviral effect or cause immune-mediated pathology, depending on the stage of gestation when IFN-λ signaling occurs (21). Interestingly, the protective and pathogenic effects of IFN-λ occurred through signaling in maternal immune cells rather than in fetal or placental tissues. In contrast, and in the setting of maternal immunocompetence, mitochondrial antiviral-signaling protein (MAVS)-dependent type I IFN signaling in the fetus was found to be necessary to restrict ZIKV infection in the fetal compartment of the placenta (48). Here we observe ZIKV strain- and dose-dependent RLR-mediated activation of the IFN response at the MFI and identify a significant fetal IFN response that correlates with fetal resorption.

When the ZIKV genome is replicated in the cytoplasm of a host cell it produces multiple ssRNA and dsRNA intermediates. These ZIKV vRNAs are primarily recognized by RIG-I, which recognizes the 5’ region of the ZIKV genome, which triggers the production of type I IFN and proinflammatory cytokines (41, 42). RNA binding triggers a confirmation change in RIG-I that

promotes interaction with MAVS. Viral sensing via RIG-I and downstream signaling via MAVS are transiently induced by the host to restrict viral replication (48, 49). However, if vRNA persists, the host is inundated with an aberrant RIG-I-driven IFN response and this prolonged RIG-I signalling can trigger immunopathology (50–52). We had therefore posited that prolonged RIG-I sensing of ZIKV vRNA may be an important driver of adverse pregnancy outcomes during ZIKV infections, possibly due to increased type I IFN production (53–55). Indeed, our results showed significant enrichment for IFN responses in the decidua and placenta prior to significant fetal resorption, with positive correlation between ZIKV vRNA load and IFN-stimulated genes, but not *Tlr3* or the proinflammatory cytokine *Il1a*. However, chemical inhibition of RIG-I in the MFI via RIG012 treatment had no effect on the rate of fetal resorption following inoculation with 10^3 PFU ZIKV-BRA, suggesting that inhibition of RIG-I signalling in the MFI is not sufficient to protect the feto-placental unit—at least at the doses tested here. Critically, results may have differed had we been able to achieve more robust inhibition of RIG-I signalling. However, this was not possible because of RIG012-associated toxicity at higher doses. We chose not to investigate this phenomenon in RIG-I knockout mice because complete ablation of RIG-I sensing could result in uncontrolled viral replication in the dam, thus failing to recapitulate the specific mechanism of fetal harm observed herein. A possible useful alternative could involve using breeding schemes involving *Ddx58*$^{-/-}$ mice (note that the *Ddx58* gene encodes murine *Rig-i*) crossed with *Ifnar1*$^{+/+}$, *Ifnar1*$^{+/-}$, and *Ifnar1*$^{-/-}$ mice. This may help better disentangle the role of RLR-driven immunopathology at the MFI and subsequent fetal demise, however it is important to note that of number of *Ddx58*$^{-/-}$ mouse models are embryo lethal (56) or develop spontaneous colitis from commensal viruses (57–59) and therefore would not be suitable for examining pathologic outcomes following ZIKV-infection during pregnancy.

Another possible explanation for differences in fetal outcomes observed between treatment groups could be that ZIKV vRNA also binds TLRs that, in turn, activate IFN responses (60);

however, recent work determined that TLR7/8, TLR9, MyD88, STING are not substantially involved in antiviral activity in the fetus and placenta (48). And, surprisingly, *MyD88*$^{-/-}$ fetuses (downstream of TLR7/8 and TLR9) resulted in lower viral burden in the decidua and placenta than those with intact *MyD88* (48). In contrast, binding of TLR3 by ZIKV vRNA suppresses the RIG-I-driven IFN response and promotes viral replication (61). Importantly, we observed inconsistent and incomplete differential activation of TLR pathways during pathologic ZIKV infections (10^5 PFU ZIKV-MEX and 10^3 PFU ZIKV-BRA). We therefore maintain that RIG-I-mediated IFN activation is a more likely mediator of fetal resorption in the *Ifnar1*$^{-/-}$ model.

Because resorbed fetuses had significantly higher ZIKV vRNA loads and relative levels of the interferon-stimulated genes *Rsad1, Ifnb,* and *Mx1* compared to normal fetuses and normal and resorbed placentas, we speculate that the fetal, rather than the placental, immune response is an important driver of fetal resorption. Indeed, Fetal Inflammatory Response Syndrome is known to be caused by systemic activation of fetal IFNs and this can result in neurological complications or death (62, 63) similar to what has been observed from infections with teratogenic pathogens like ZIKV, but more studies are needed to understand the relative importance of fetal-derived immune responses. As previously mentioned, a prior study found that *Ifnar1*$^{-/-}$ fetuses were protected from fetal resorption while *Ifnar1*$^{+/-}$ fetuses were not (17), but the fetal IFN response was not examined so its contribution to fetal resorption in that system remains unknown. Further, in an immunocompetent mouse model, the IFN response was more robust in fetal endothelial cells compared to placental cells (48), suggesting that the magnitude of the response may determine its contribution to resorption.

While the IFN response appears to be a primary mediator of fetal demise in the *Ifnar1*$^{-/-}$ model, it is important to consider the possibility that this phenotype is multifactorial. For example, the 10^5 PFU ZIKV-MEX placenta transcriptome had significant enrichment for MYC targets V1, hypoxia, and epithelial mesenchymal transition compared to 10^3 ZIKV-BRA. MYC targets V1 are

associated with cell proliferation (64), suggesting that 10^5 PFU ZIKV-MEX placentas experienced greater tissue growth compared to 10^3 ZIKV-BRA. Because cell proliferation is closely linked with apoptosis (65), enrichment for MYC targets V1 may indicate compensation for cell death that is occurring. In fact, enrichment for MYC targets V1 was observed in all of our ZIKV-inoculated groups when compared to PBS. Hypoxia-induced changes in metabolism drive placentation in mice and humans (66), however after placentation, hypoxia conditions can increase inflammation through release of damage-associated molecular patterns (DAMPs)(67). At certain levels, inflammation and DAMPs increase the risk of intrauterine growth restriction and stillbirth, even in the absence of a pathogen(67). Murine placentation is complete at E10.5, suggesting that enrichment for hypoxia in the E11.5 placenta is detrimental (68). Enrichment for epithelial mesenchymal transition suggests a greater presence of migratory cells (69), which is critical for formation of the labyrinth and gastrulation (68). Poor labyrinth formation would impact nutrient and gas exchange between mother and fetus (70), which could result in intrauterine growth restriction and fetal death. Abnormal gastrulation would impact cell type and location during embryo development (71), which could result in an improperly formed embryo. While these signatures may be secondary to a robust IFN response induced by ZIKV-MEX and ZIKV-BRA, they have important implications for potential concurrent mechanisms of fetal resorption.

ZIKV-MEX and ZIKV-BRA are genetically very similar, but differences observed in fetal outcomes between the two strains may be due to virus genetic determinants of virulence. The seven amino acid differences between them occur in the NS1, NS3, and NS5 proteins (**Table 1**). ZIKV NS1 disrupts endothelial barrier function (72), which is particularly important at the placenta because endothelial cells remodel the maternal and fetal placental vasculature. Abnormalities in placental endothelial cells lead to high rates of apoptosis, and subsequent fetal growth restriction and pre-eclampsia (73). It is possible that ZIKV-BRA may produce higher levels of NS1 compared to ZIKV-MEX and therefore may be more adept at disrupting

endothelial barriers, thus contributing to significantly higher rates of fetal resorption—but we did not test that here. This could also explain why ZIKV-MEX is capable of causing fetal demise at higher doses. ZIKV NS3 binds dsRNA replication intermediates and associates with NS5 to promote genome replication, and mutations in the ATPase or RNA-binding region of ZIKV NS3 have both been shown to alter helicase activity and reduce genome replication (74). Therefore, it is possible that differences in NS3 helicase activity between the two strains may explain the different ZIKV vRNA loads observed in the decidua, placenta, and fetus. Further, ZIKV NS3 has been associated with brain calcifications in ZIKV-infected fetuses (75), demonstrating that the overall activity and concentration of ZIKV NS3 can be associated with adverse outcomes.

Importantly, CD8 T cell epitopes are located in NS1, NS3, and NS5 (76). Therefore, polymorphisms at these sites between ZIKV-MEX and ZIKV-BRA may alter T cell activation, including differentially inducing cytotoxic CD8 T cells, but more studies are needed to investigate this. During congenital infection and/or hyperinflammatory states, maternal and fetal CD8 T cells infiltrate the MFI (77, 78). ZIKV activation of CD8 T cells has been associated with significant IFN gamma, TNF alpha, and granzyme B production (79–81), all of which are cytotoxic, despite being required to control ZIKV infection (76, 82). CD8 T cells induce cytotoxic effects in response to ZIKV in immunologically privileged spaces like the neuronal cavity (83), but their role at the MFI remains unknown. Other congenital infections, including human cytomegalovirus, induce maternal- and fetal-derived CD8 T cell-mediated cytotoxic effects in the placenta (78, 84, 85), and can even mediate allogeneic intolerance (86). In fact, one study found that ZIKV-infected placentas from fetuses with microcephaly had increased T cell activation, suggesting that T cell activation plays a role in the severity of CZS (87). Future work should consider how T cells, particularly CD8 T cells, mediate pathology during ZIKV-infected pregnancies. The future spread of ZIKV will remain a threat to pregnant people in many locations around the globe. While the exact mechanism underlying ZIKV-induced fetal harm

616 remains unclear, these studies highlight that RIG-I can mediate a pathologic IFN response at
617 the MFI and that the fetal immune response may be an underappreciated contributor to adverse
618 pregnancy outcomes during ZIKV infections.

METHODS

Ethical approval. This study was approved by the University of Minnesota, Twin Cities Institutional Animal Care and Use Committee (Animal Care and Use protocol number 2401-41654A).

Cells and Viruses

African green monkey kidney cells (Vero cells; ATCC CCL-81) were maintained in Dulbecco's modified Eagle medium (DMEM) supplemented with 10% fetal bovine serum (FBS; Corning, Manassas, VA), 1× Antibiotic Antimycotic solution (Corning, Manassas, VA) and incubated at 37°C in 5% CO2. *Aedes albopictus* mosquito cells (C6/36; ATCC CRL-1660) were maintained in DMEM supplemented with 10% fetal bovine serum (FBS; HyClone, Logan, UT), 2 mM L-glutamine, 1.5 g/liter sodium bicarbonate, 1× Antibiotic Antimycotic solution, and incubated at 28°C in 5% CO2. The cell lines were obtained from the American Type Culture Collection, were not further authenticated, and were not specifically tested for mycoplasma. ZIKV strain R116265 (ZIKV-MEX; GenBank KX766029) was originally isolated from a 73-year-old-male traveling in Mexico in 2016 with a single round of amplification on Vero cells (CDC, Ft. Collins, CO). ZIKV strain Paraiba_01 (ZIKV-BRA; GenBank KX280026) was originally isolated from human serum in Brazil in 2015 with two rounds of amplification on Vero cells, and a master stock was obtained from Kevin Noguchi at Washington University in St. Louis (St. Louis, MO). Virus challenge stocks were prepared by inoculation onto a confluent monolayer of C6/36 mosquito cells. Virus challenge stocks were sequence authenticated as described in reference (18).

Plaque Assay

Quantification of virus titer in maternal serum, placenta, and fetuses were completed by plaque assay on Vero cells. Duplicate wells were infected with 0.1 ml aliquots from serial 10-fold dilutions in growth medium and virus was adsorbed for 1 h. After incubation, the monolayers

were overlaid with 3 ml containing a 1:1 mixture of 1.2% oxoid agar and 2× DMEM (Gibco, Carlsbad, CA) with 10% (vol/vol) FBS and 2% (vol/vol) Antibiotic Antimycotic solution. Cells were incubated at 37°C in 5% CO2 for 3 days (ZIKV-BRA) or 5 days (ZIKV-MEX) for plaque development. Cell monolayers were then stained with 3 ml of overlay containing a 1:1 mixture of 1.2% oxoid agar with 4% neutral red (Gibco) and 2× DMEM with 2% (vol/vol) FBS, and 2% (vol/vol) Antibiotic Antimycotic solution. Cells were incubated overnight at 37°C in 5% CO2 and plaques were counted.

Mice

Female *Ifnar1*$^{-/-}$ mice on the C57BL/6 background were bred in the specific pathogen-free animal facilities of the University of Minnesota within the College of Veterinary Medicine. Male C57BL/6 mice were purchased from Jackson Laboratories. Timed matings between female *Ifnar1*$^{-/-}$ mice and male C57BL/6 mice resulted in *Ifnar1*$^{+/-}$ progeny.

Subcutaneous Inoculation

All pregnant dams were between 6 and 10 weeks of age and were randomly assigned to infected or control groups. Matings between *Ifnar1*$^{-/-}$ dams and wild-type sires were timed by checking for the presence of a vaginal plug, indicating gestational age E0.5. At embryonic day 7.5 (E7.5) dams were inoculated in the right hind footpad with 1×10^3 or 1×10^5 PFU of the selected ZIKV strain in sterile phosphate-buffered saline (PBS) or with sterile PBS alone to serve as experimental controls. All animals were closely monitored by laboratory staff for adverse reactions and/or clinical signs of disease. A submandibular blood draw was performed at 2, 4, 7 and/or 10 days post inoculation (dpi), and serum was collected to verify viremia. Mice were humanely euthanized and necropsied at E9.5, E11.5, E14.5, or E17.5.

Intraperitoneal administration of RIG012

RIG012 (MedChemExpress, Monmouth Junction, NJ) was dissolved in sterile DMSO at a concentration of 30mg/mL before being mixed with an equal volume of Tween 80 and stored at 4°C. Mice were weighed and doses were calculated. The RIG012 in DMSO/Tween 80 solution was diluted with nine parts sterile water immediately prior to injection to make a final concentration of 5/5/90 (DMSO/Tween 80/H_2O) which was dosed at 15uL/g to provide a dose of 22.5mg/kg. A control solution of 5/5/90 (DMSO/Tween 80/H_2O) was dosed at 15uL/g. Animals were intraperitoneally injected using a 28G needle with a 1mL syringe. Animals were monitored for signs of toxicity for up to 1 hour post injection, and every 12 hours following injection.

Mouse necropsy

Following inoculation with ZIKV or PBS, mice were sacrificed at E9.5, E11.5, E14.5, or E17.5. Tissues were carefully dissected using sterile instruments that were changed between each mouse to minimize possible cross contamination. Each organ and neonate was morphologically evaluated *in situ* prior to removal. Using sterile instruments, the uterus was removed and dissected to remove individual concepti. Each conceptus was placed in a sterile culture dish and dissected to separate the fetus and the maternal-fetal interface (MFI) for gross evaluation. Fetuses were characterized as “normal” or “resorbed,” with the latter being defined as having significant growth retardation and reduced physiological structure compared to littermates and controls, accompanied by clearly evident developmental delay or visualization of a macroscopic plaque in the uterus. The MFI included maternal-derived decidua tissue and fetal-derived placental tissue. At E9.5 and E11.5, the MFI was further dissected under a stereoscope to separate decidua and placenta tissues. Tissues isolated at E9.5, E11.5, and E17.5 were snap frozen in RNase-free tubes on dry ice. Tissues isolated at E14.5 were snap frozen as described or frozen in PBS supplemented with 20% FBS and 1% Antibiotic Antimycotic. A subset of

tissues from each timepoint were fixed in 10% neutral buffered formalin for 24 to 96 hours (depending on tissue mass) then transferred to 70% ethanol until imaged.

Crown-to-rump length

Crown-to-rump length (CRL) was measured by tracing the distance from the crown of the head to the base of the tail, using ImageJ. Resorbed fetuses were excluded from measurement analyses because they would not survive if the pregnancy was allowed to progress to term (19).

Fetal and MFI viral titers

An Omni TH115 homogenizer (Omni International, Kennesaw, GA) was used to homogenize fetus and MFI samples following necropsy. Samples were submerged in chilled PBS supplemented with 20% FBS and 1% Antibiotic Antimycotic solution in 2 ml Safelock tubes (Eppendorf, Hamburg, Germany). Omni soft tissue probes (Omni International, Kennesaw, GA) were used to homogenize samples at medium speed. Homogenized samples were clarified by centrifugation at 10,000 × *g* for 2 min. The supernatant was removed and 0.1 ml was immediately plated in duplicate for plaque assay. The remainder was stored at −80°C.

Determination of fetal sex

DNA was extracted and purified from E9.5 and E11.5 fetuses using a Zymo Quick-DNA miniprep plus kit (Zymo Research, Irvine, CA) or Maxwell RSC Tissue DNA kit (Promega, Madison, WI). PCR and gel electrophoresis were conducted as previously described (88).

Total RNA extraction

Total RNA was extracted and purified from deciduas, placentas, and fetuses using a Direct-zol RNA miniprep kit (Zymo Research, Irvine, CA). RNA was eluted in 50 to 100uL RNase-free water. RNA concentration and purity were measured by a Qubit 4 fluorometer (ThermoFisher, Waltham, MA).

Quantification of vRNA load

Viral RNA was quantified from extracted total RNA from maternal-fetal tissues by quantitative reverse transcription-PCR as described previously (18, 19, 89). Total RNA was titrated by qRT-PCR using TaqMan Fast virus 1-step master mix (Applied Biosystems, Waltham, MA) on a QuantStudio3 (ThermoFisher, Waltham, MA). ZIKV RNA titers were interpolated from a standard curve of diluted in vitro-transcribed ZIKV RNA. The limit of detection for this assay is 150 ZIKV genome copies/ml (1.60 log10 copies/tissue).

Illumina RNAseq library preparation and sequencing

Multiplex sequencing libraries were generated from 500 ng of total RNA (per library) using Illumina's TruSeq sample prep kit and multiplexing sample preparation oligonucleotide kit (Illumina Inc., San Diego, CA) following the manufacturer's instructions. Up to four samples per tissue per animal per inoculation group, with equal proportions male and female, were submitted for sequencing. Samples were sequenced on an Illumina NovaSeq, which generated 2x150 bp paired-end reads at a depth of 20 million reads. Illumina's bcl2fastq v2.20 was used for de-multiplexing, and sequence quality was assessed based on %GC content, average base quality, and sequence duplication levels.

Sequence alignment and transcript quantification

RNA sequencing data were quality-checked using FastQC (v0.11.9)(90) and summarized using MultiQC (v1.12)(91). The resulting trimmed reads were aligned to the *Mus musculus* genome [Mus_musculus.GRCm39.cdna.all.index] using kallisto (v0.46.1)(92), which relies on a pseudoalignment framework. Out of 3.7 billion sequence reads, 73–93% of reads mapped unambiguously to the *Mus musculus* reference genome. Downstream analysis followed the DIY Transcriptomics R workflow (93) in R (v4.2.3), supplemented by Pathview analysis (40). Aligned reads were annotated using the tximport (v1.28.0) R package (94). Differentially expressed genes were identified using raw gene counts. Differential gene expression analysis was

performed using the DESeq2 package (v1.40.1)(37) using a significance cutoff of 0.05 and a fold change cutoff of 1 $\log_2$ fold change. Volcano plots, temporal plots, and heatmaps were generated using the ggplot2 package (v3.4.2) in R (95). Gene Set Enrichment Analysis was performed using GSEA (v4.3.2)(39) on normalized data against Hallmark gene sets available from MSigDB (Mouse MSigDB Collections 2004). All data processing and analysis scripts are publicly available on GitHub (https://github.com/aliotalab/ZIKVplacentaRNAseq/tree/main).

Quantification of RIG012 in serum and maternal-fetal interface (MFI) tissue

5 µL plasma samples were directly loaded to a 96-well Millipore Multiscreen Solvinert 0.45 micron low binding PTFE hydrophilic filter plate. MFI samples were homogenized with water (x3 dilution) then 5 µL was loaded to the filter plate. All plasma/tissue samples were treated with 75 µL 90/10 acetonitrile/water with Atorvastatin as I.S. to extract the analyte and precipitate protein. The plates were agitated on ice for approximately ten minutes prior to centrifugation into a collection plate. Separate standard curves were prepared in blank mouse plasma and tissue homogenate and processed in parallel with the samples. The filtrate was directly analyzed by LC-MS/MS analysis against. HPLC and MS/MS parameters are provided in the accompanying tables (**Table 4 - Table 6**).

Compound	RIG012	I.S. (Atorvastin)
Column	Thermo Betasil C18 5µ, 50x2.1mm	
Mobile phase	A: Water with 0.1% Formic Acid B: Acetonitrile with 0.1% Formic Acid	
Flow rate (ml/min)	0.35	
Temperature (°C)	35	
Injection volume (µl)	10	

Table 4: LC (Shimadzu UFLC XR) conditions

Time (min)	Mobile phase A (%)	Mobile phase B (%)
0.2	90	10
0.5	90	10
2.0	5	95
3.0	5	95
4.0	90	10
5.9	90	10

Table 5: Gradient elution conditions

Compound	RIG012	I.S. (Atorvastatin)
MRM(-)	359.4/268.2	557.1/397
Collision Gas	Low	
Curtain GAS	30	
Ion Source Gas1	55	
Ion Source Gas2	55	
Ion Spray Voltage	-4500	
Temperature (°C)	550	
Collision Energy	-26	-50
Declustering Potential	-75	-75
Entrance Potential	-10	
Collision Cell Exit Potential	-10	

Table 6: MS (API6500+) conditions

Gene Expression of RIG-I-induced genes

RNA was extracted and purified from placentas using a Direct-zol RNA kit (Zymo Research). The High-Capacity RNA-to-cDNA kit (Applied Biosystems) was used to synthesize cDNA. Quantitative PCR using Fast Advanced Master Mix (TaqMan) was used to quantify RIG-I-induced genes on a QuantStudio3 (Applied Biosystems). The following TaqMan assays were used: *Hprt* (Mm00446968_m1), *Ifnb* (Mm00439552_s1), *Rsad2* (Mm00491265_m1), and *Mx1*

(Mm00487796_m1). *Ifnb*, *Rsad2*, and *Mx1* were normalized to *Hprt* and then the threshold cycle value (2-delta delta C_T) was calculated relative to Vehicle/PBS controls.

Statistical analyses

All statistical analyses from the pathology data were conducted using GraphPad Prism 9 (GraphPad Software, CA, USA) or RStudio (Posit Software, PBC, Boston, MA, USA). Statistical analyses from the transcriptomic data were conducted in RStudio, under the null hypothesis of equal gene expression between groups. Statistical significance was designated to P-values of less than 0.05.

Data availability

Raw Illumina sequencing data are available on the NCBI Sequence Read Archive under BioProject no. **SUB15084024** (https://www.ncbi.nlm.nih.gov/bioproject/**SUB15084024**). All data processing and analysis scripts are publicly available on GitHub (https://github.com/aliotalab/ZIKVplacentaRNAseq/tree/main).

ACKNOWLEDGEMENTS

We thank the University of Minnesota's Genomics Center for RNA sequencing and the Minnesota Supercomputing Institute for computing resources. We thank Dr. Vivian Bardwell for training on early gestation necropsies and Dr. Micah Gearhart for advising on bioinformatic analysis. We thank Dr. Grace Vaziri for her critical review of the manuscript.

FUNDING STATEMENT

Funding for this project came from National Institutes of Health grants R01AI132563 to M.T.A. E.K.B was supported by the University of Minnesota, Twin Cities, Institute for Molecular Virology Training Program predoctoral fellowship number T32AI083196. The pharmacokinetic data were acquired by a mass spectrometer funded by NIH grant 1 S10OD030332-01 (M.D.C.). The publication's contents are solely the responsibility of the authors and do not necessarily represent the official views of the NIH. The funders had no role in study design, data collection and analysis, decision to publish, or preparation of the manuscript.

REFERENCES

1. Ander SE, Diamond MS, Coyne CB. 2019. Immune responses at the maternal-fetal interface. Sci Immunol 4.
2. Sheridan MA, Yunusov D, Balaraman V, Alexenko AP, Yabe S, Verjovski-Almeida S, Schust DJ, Franz AW, Sadovsky Y, Ezashi T, Roberts RM. 2017. Vulnerability of primitive human placental trophoblast to Zika virus. Proc Natl Acad Sci U A 114:E1587–E1596.
3. Cao B, Diamond MS, Mysorekar IU. 2017. Maternal-fetal transmission of Zika virus: Routes and signals for infection. J Interferon Cytokine Res 37:287–294.
4. Coyne CB, Lazear HM. 2016. Zika virus - reigniting the TORCH. Nat Rev Microbiol 14:707–715.
5. Weisblum Y, Oiknine-Djian E, Vorontsov OM, Haimov-Kochman R, Zakay-Rones Z, Meir K, Shveiky D, Elgavish S, Nevo Y, Roseman M, Bronstein M, Stockheim D, From I, Eisenberg I, Lewkowicz AA, Yagel S, Panet A, Wolf DG. 2017. Zika Virus Infects Early- and Midgestation Human Maternal Decidual Tissues, Inducing Distinct Innate Tissue Responses in the Maternal-Fetal Interface. J Virol 91.
6. Noronha L de, Zanluca C, Azevedo MLV, Luz KG, Santos CNDD. 2016. Zika virus damages the human placental barrier and presents marked fetal neurotropism. Mem Inst Oswaldo Cruz 111:287–293.
7. Koenig MR, Mitzey AM, Zeng X, Reyes L, Simmons HA, Morgan TK, Bohm EK, Pritchard JC, Schmidt JA, Ren E, Leyva Jaimes FB, Winston E, Basu P, Weiler AM, Friedrich TC, Aliota MT, Mohr EL, Golos TG. 2023. Vertical transmission of African-lineage Zika virus through the fetal membranes in a rhesus macaque (Macaca mulatta) model. PLoS Pathog 19:e1011274.
8. Koenig MR, Mitzey AM, Morgan TK, Zeng X, Simmons HA, Mejia A, Leyva Jaimes F, Keding LT, Crooks CM, Weiler AM, Bohm EK, Aliota MT, Friedrich TC, Mohr EL, Golos TG. 2023. Infection of the maternal-fetal interface and vertical transmission following low-dose inoculation of pregnant rhesus macaques (Macaca mulatta) with an African-lineage Zika virus. PLoS One 18:e0284964.

9. Bhatnagar J, Rabeneck DB, Martines RB, Reagan-Steiner S, Ermias Y, Estetter LBC, Suzuki T, Ritter J, Keating MK, Hale G, Gary J, Muehlenbachs A, Lambert A, Lanciotti R, Oduyebo T, Meaney-Delman D, Bolaños F, Saad EAP, Shieh W-J, Zaki SR. 2017. Zika Virus RNA Replication and Persistence in Brain and Placental Tissue. Emerg Infect Dis 23:405–414.
10. Charlier C, Beaudoin M-C, Couderc T, Lortholary O, Lecuit M. 2017. Arboviruses and pregnancy: maternal, fetal, and neonatal effects. Lancet Child Adolesc Health 1:134–146.
11. Calvet G, Aguiar RS, Melo ASO, Sampaio SA, de Filippis I, Fabri A, Araujo ESM, de Sequeira PC, de Mendonça MCL, de Oliveira L, Tschoeke DA, Schrago CG, Thompson FL, Brasil P, Dos Santos FB, Nogueira RMR, Tanuri A, de Filippis AMB. 2016. Detection and sequencing of Zika virus from amniotic fluid of fetuses with microcephaly in Brazil: a case study. Lancet Infect Dis 16:653–660.
12. Peña F, Pimentel R, Khosla S, Mehta SD, Brito MO. 2019. Zika Virus Epidemic in Pregnant Women, Dominican Republic, 2016-2017. Emerg Infect Dis 25:247–255.
13. de Oliveira DN, Lima EO, Melo CFOR, Delafiori J, Guerreiro TM, Rodrigues RGM, Morishita KN, Silveira C, Muraro SP, de Souza GF, Vieira A, Silva A, Batista RF, Doriqui MJR, Sousa PS, Milanez GP, Proença-Módena JL, Cavalcanti DP, Catharino RR. 2019. Inflammation markers in the saliva of infants born from Zika-infected mothers: exploring potential mechanisms of microcephaly during fetal development. Sci Rep 9:13606.
14. Vinhaes CL, Arriaga MB, de Almeida BL, Oliveira JV, Santos CS, Calcagno JI, Carvalho TX, Giovanetti M, Alcantara LCJ, de Siqueira IC, Andrade BB. 2020. Newborns With Zika Virus-Associated Microcephaly Exhibit Marked Systemic Inflammatory Imbalance. J Infect Dis 222:670–680.
15. Hunt K, Kennedy SH, Vatish M. 2016. Definitions and reporting of placental insufficiency in biomedical journals: a review of the literature. Eur J Obstet Gynecol Reprod Biol 205:146–149.
16. Azamor T, Cunha DP, Nobre Pires KS, Lira Tanabe EL, Melgaço JG, Vieira da Silva AM, Ribeiro-Alves M, Calvo TL, Tubarão LN, da Silva J, Fernandes CB, Fonseca de Souza A,

Torrentes de Carvalho A, Avvad-Portari E, da Cunha Guida L, Gomes L, Lopes Moreira ME, Dinis Ano Bom AP, Cristina da Costa Neves P, Missailidis S, Vasconcelos Z, Borbely AU, Moraes MO. 2024. Decidual production of interferon lambda in response to ZIKV persistence: Clinical evidence and in vitro modelling. Heliyon 10:e30613.

17. Yockey LJ, Jurado KA, Arora N, Millet A, Rakib T, Milano KM, Hastings AK, Fikrig E, Kong Y, Horvath TL, Weatherbee S, Kliman HJ, Coyne CB, Iwasaki A. 2018. Type I interferons instigate fetal demise after Zika virus infection. Sci Immunol 3.
18. Bohm EK, Vangorder-Braid JT, Jaeger AS, Moriarty RV, Baczenas JJ, Bennett NC, O'Connor SL, Fritsch MK, Fuhler NA, Noguchi KK, Aliota MT. 2021. Zika virus infection of pregnant Ifnar1-/- mice triggers strain-specific differences in fetal outcomes. J Virol JVI0081821.
19. Jaeger AS, Murrieta RA, Goren LR, Crooks CM, Moriarty RV, Weiler AM, Rybarczyk S, Semler MR, Huffman C, Mejia A, Simmons HA, Fritsch M, Osorio JE, Eickhoff JC, O'Connor SL, Ebel GD, Friedrich TC, Aliota MT. 2019. Zika viruses of African and Asian lineages cause fetal harm in a mouse model of vertical transmission. PLoS Negl Trop Dis 13:e0007343.
20. Yu W, Zhang B, Hong X, Cai H, Wang Y, Lu J, Hu X, Cao B. 2023. Identification of desoxyrhapontigenin as a novel antiviral agent against congenital Zika virus infection. Antivir Res 211:105542.
21. Casazza RL, Philip DT, Lazear HM. 2022. Interferon Lambda Signals in Maternal Tissues to Exert Protective and Pathogenic Effects in a Gestational Stage-Dependent Manner. MBio 13:e0385721.
22. Azamor T, Cunha DP, da Silva AMV, Bezerra OC de L, Ribeiro-Alves M, Calvo TL, Kehdy F de SG, Manta FS de N, Pinto TG de T, Ferreira LP, Portari EA, Guida L da C, Gomes L, Moreira MEL, de Carvalho EF, Cardoso CC, Muller M, Ano Bom APD, Neves PC da C, Vasconcelos Z, Moraes MO. 2021. Congenital Zika Syndrome Is Associated With Interferon Alfa Receptor 1. Front Immunol 12:764746.

23. Foo S-S, Chen W, Chan Y, Lee W-S, Lee S-A, Cheng G, Nielsen-Saines K, Brasil P, Jung JU. 2018. Biomarkers and immunoprofiles associated with fetal abnormalities of ZIKV-positive pregnancies. JCI Insight 3.

24. Lanciotti RS, Lambert AJ, Holodniy M, Saavedra S, Signor LDCC. 2016. Phylogeny of Zika Virus in Western Hemisphere, 2015. Emerg Infect Dis 22:933–935.

25. Pimentel R, Khosla S, Rondon J, Peña F, Sullivan G, Perez M, Mehta SD, Brito MO. 2021. Birth Defects and Long-Term Neurodevelopmental Abnormalities in Infants Born During the Zika Virus Epidemic in the Dominican Republic. Ann Glob Health 87:4.

26. Cauchemez S, Besnard M, Bompard P, Dub T, Guillemette-Artur P, Eyrolle-Guignot D, Salje H, Van Kerkhove MD, Abadie V, Garel C, Fontanet A, Mallet H-P. 2016. Association between Zika virus and microcephaly in French Polynesia, 2013–15: a retrospective study. Lancet 387:2125–2132.

27. Rice ME, Galang RR, Roth NM, Ellington SR, Moore CA, Valencia-Prado M, Ellis EM, Tufa AJ, Taulung LA, Alfred JM, Pérez-Padilla J, Delgado-López CA, Zaki SR, Reagan-Steiner S, Bhatnagar J, Nahabedian JF 3rd, Reynolds MR, Yeargin-Allsopp M, Viens LJ, Olson SM, Jones AM, Baez-Santiago MA, Oppong-Twene P, VanMaldeghem K, Simon EL, Moore JT, Polen KD, Hillman B, Ropeti R, Nieves-Ferrer L, Marcano-Huertas M, Masao CA, Anzures EJ, Hansen RL Jr, Pérez-Gonzalez SI, Espinet-Crespo CP, Luciano-Román M, Shapiro-Mendoza CK, Gilboa SM, Honein MA. 2018. Vital Signs: Zika-Associated Birth Defects and Neurodevelopmental Abnormalities Possibly Associated with Congenital Zika Virus Infection - U.S. Territories and Freely Associated States, 2018. MMWR Morb Mortal Wkly Rep 67:858–867.

28. Nogueira ML, Nery Júnior NRR, Estofolete CF, Bernardes Terzian AC, Guimarães GF, Zini N, Alves da Silva R, Dutra Silva GC, Junqueira Franco LC, Rahal P, Bittar C, Carneiro B, Vasconcelos PFC, Freitas Henriques D, Barbosa DMU, Lopes Rombola P, de Grande L, Negri Reis AF, Palomares SA, Wakai Catelan M, Cruz LEAA, Necchi SH, Mendonça RCV, Penha Dos Santos IN, Alavarse Caron SB, Costa F, Bozza FA, Soares de Souza A, Brandão de

Mattos CC, de Mattos LC, Vasilakis N, Oliani AH, Vaz Oliani DCM, Ko AI. 2018. Adverse birth outcomes associated with Zika virus exposure during pregnancy in São José do Rio Preto, Brazil. Clin Microbiol Infect 24:646–652.

29. Ximenes RA de A, Miranda-Filho D de B, Montarroyos UR, Martelli CMT, Araújo TVB de, Brickley E, Albuquerque M de FPM de, Souza WV, Ventura LO, Ventura CV, Gois AL, Leal MC, Oliveira DM da S, Eickmann SH, Carvalho MDCG, Silva PFS da, Rocha MAW, Ramos RCF, Brandão-Filho SP, Cordeiro MT, Bezerra LCA, Dimech G, Valongueiro S, Pires P, Castanha PM da S, Dhalia R, Marques-Júnior ETA, Rodrigues LC, Microcephaly Epidemic Research Group (MERG). 2021. Zika-related adverse outcomes in a cohort of pregnant women with rash in Pernambuco, Brazil. PLoS Negl Trop Dis 15:e0009216.
30. Brasil P, Pereira JP Jr, Moreira ME, Ribeiro Nogueira RM, Damasceno L, Wakimoto M, Rabello RS, Valderramos SG, Halai U-A, Salles TS, Zin AA, Horovitz D, Daltro P, Boechat M, Raja Gabaglia C, Carvalho de Sequeira P, Pilotto JH, Medialdea-Carrera R, Cotrim da Cunha D, Abreu de Carvalho LM, Pone M, Machado Siqueira A, Calvet GA, Rodrigues Baião AE, Neves ES, Nassar de Carvalho PR, Hasue RH, Marschik PB, Einspieler C, Janzen C, Cherry JD, Bispo de Filippis AM, Nielsen-Saines K. 2016. Zika Virus Infection in Pregnant Women in Rio de Janeiro. N Engl J Med 375:2321–2334.
31. Barbeito-Andrés J, Schuler-Faccini L, Garcez PP. 2018. Why is congenital Zika syndrome asymmetrically distributed among human populations? PLoS Biol 16:e2006592.
32. Jaeger AS, Weiler AM, Moriarty RV, Rybarczyk S, O'Connor SL, O'Connor DH, Seelig DM, Fritsch MK, Friedrich TC, Aliota MT. 2020. Spondweni virus causes fetal harm in Ifnar1-/- mice and is transmitted by Aedes aegypti mosquitoes. Virology 547:35–46.
33. Sones JL, Davisson RL. 2016. Preeclampsia, of mice and women. Physiol Genomics 48:565–572.

34. Miner JJ, Cao B, Govero J, Smith AM, Fernandez E, Cabrera OH, Garber C, Noll M, Klein RS, Noguchi KK, Mysorekar IU, Diamond MS. 2016. Zika Virus Infection during Pregnancy in Mice Causes Placental Damage and Fetal Demise. Cell 165:1081–1091.
35. Payne S. 2017. Introduction to RNA Viruses. Viruses 97.
36. Flores LE, Hildebrandt TB, Kühl AA, Drews B. 2014. Early detection and staging of spontaneous embryo resorption by ultrasound biomicroscopy in murine pregnancy. Reprod Biol Endocrinol 12:38.
37. Love MI, Huber W, Anders S. 2014. Moderated estimation of fold change and dispersion for RNA-seq data with DESeq2. Genome Biol 15:550.
38. Liberzon A, Birger C, Thorvaldsdóttir H, Ghandi M, Mesirov JP, Tamayo P. 2015. The Molecular Signatures Database (MSigDB) hallmark gene set collection. Cell Syst 1:417–425.
39. Subramanian A, Tamayo P, Mootha VK, Mukherjee S, Ebert BL, Gillette MA, Paulovich A, Pomeroy SL, Golub TR, Lander ES, Mesirov JP. 2005. Gene set enrichment analysis: a knowledge-based approach for interpreting genome-wide expression profiles. Proc Natl Acad Sci U A 102:15545–15550.
40. Luo W, Brouwer C. 2013. Pathview: an R/Bioconductor package for pathway-based data integration and visualization. Bioinformatics 29:1830–1831.
41. Hertzog J, Dias Junior AG, Rigby RE, Donald CL, Mayer A, Sezgin E, Song C, Jin B, Hublitz P, Eggeling C, Kohl A, Rehwinkel J. 2018. Infection with a Brazilian isolate of Zika virus generates RIG-I stimulatory RNA and the viral NS5 protein blocks type I IFN induction and signaling. Eur J Immunol 48:1120–1136.
42. Chazal M, Beauclair G, Gracias S, Najburg V, Simon-Lorière E, Tangy F, Komarova AV, Jouvenet N. 2018. RIG-I Recognizes the 5’ Region of Dengue and Zika Virus Genomes. Cell Rep 24:320–328.
43. Rawling DC, Jagdmann GE Jr, Potapova O, Pyle AM. 2020. Small-Molecule Antagonists of the RIG-I Innate Immune Receptor. ACS Chem Biol 15:311–317.

44. Han VX, Patel S, Jones HF, Nielsen TC, Mohammad SS, Hofer MJ, Gold W, Brilot F, Lain SJ, Nassar N, Dale RC. 2021. Maternal acute and chronic inflammation in pregnancy is associated with common neurodevelopmental disorders: a systematic review. Transl Psychiatry 11:71.

45. Chudnovets A, Liu J, Narasimhan H, Liu Y, Burd I. 2020. Role of Inflammation in Virus Pathogenesis during Pregnancy. J Virol 95:e01381-19.

46. Kumar M, Saadaoui M, Al Khodor S. 2022. Infections and Pregnancy: Effects on Maternal and Child Health. Front Cell Infect Microbiol 12:873253.

47. Gashimova NR, Pankratyeva LL, Bitsadze VO, Khizroeva JK, Tretyakova MV, Grigoreva KN, Tsibizova VI, Gris J-C, Degtyareva ND, Yakubova FE, Makatsariya AD. 2023. Inflammation and Immune Reactions in the Fetus as a Response to COVID-19 in the Mother. J Clin Med 12:4256.

48. Alippe Y, Wang L, Coskun R, Muraro SP, Zhao FR, Elam-Noll M, White JM, Vota DM, Hauk VC, Gordon JI, Handley SA, Diamond MS. 2024. Fetal MAVS and type I IFN signaling pathways control ZIKV infection in the placenta and maternal decidua. J Exp Med 221:e20240694.

49. Zhao Z, Li Q, Ashraf U, Yang M, Zhu W, Gu J, Chen Z, Gu C, Si Y, Cao S, Ye J. 2022. Zika virus causes placental pyroptosis and associated adverse fetal outcomes by activating GSDME. Elife 11.

50. Murira A, Lamarre A. 2016. Type-I Interferon Responses: From Friend to Foe in the Battle against Chronic Viral Infection. Front Immunol 7:609.

51. Griffin DE. 2022. Why does viral RNA sometimes persist after recovery from acute infections? PLoS Biol 20:e3001687.

52. Arai Y, Yamanaka I, Okamoto T, Isobe A, Nakai N, Kamimura N, Suzuki T, Daidoji T, Ono T, Nakaya T, Matsumoto K, Okuzaki D, Watanabe Y. 2023. Stimulation of interferon-β responses by aberrant SARS-CoV-2 small viral RNAs acting as retinoic acid-inducible gene-I agonists. iScience 26:105742.

53. Major J, Crotta S, Llorian M, McCabe TM, Gad HH, Priestnall SL, Hartmann R, Wack A. 2020. Type I and III interferons disrupt lung epithelial repair during recovery from viral infection. Science 369:712–717.

54. Gürtler C, Carty M, Kearney J, Schattgen SA, Ding A, Fitzgerald KA, Bowie AG. 2014. SARM regulates CCL5 production in macrophages by promoting the recruitment of transcription factors and RNA polymerase II to the Ccl5 promoter. J Immunol Baltim Md 1950 192:4821–4832.

55. Blank T, Prinz M. 2017. Type I interferon pathway in CNS homeostasis and neurological disorders. Glia 65:1397–1406.

56. Kato H, Sato S, Yoneyama M, Yamamoto M, Uematsu S, Matsui K, Tsujimura T, Takeda K, Fujita T, Takeuchi O, Akira S. 2005. Cell type-specific involvement of RIG-I in antiviral response. Immunity 23:19–28.

57. Wang Y, Zhang H-X, Sun Y-P, Liu Z-X, Liu X-S, Wang L, Lu S-Y, Kong H, Liu Q-L, Li X-H, Lu Z-Y, Chen S-J, Chen Z, Bao S-S, Dai W, Wang Z-G. 2007. Rig-I-/- mice develop colitis associated with downregulation of G alpha i2. Cell Res 17:858–868.

58. Liu L, Gong T, Tao W, Lin B, Li C, Zheng X, Zhu S, Jiang W, Zhou R. 2019. Commensal viruses maintain intestinal intraepithelial lymphocytes via noncanonical RIG-I signaling. Nat Immunol 20:1681–1691.

59. Zhu H, Xu W-Y, Hu Z, Zhang H, Shen Y, Lu S, Wei C, Wang Z-G. 2017. RNA virus receptor Rig-I monitors gut microbiota and inhibits colitis-associated colorectal cancer. J Exp Clin Cancer Res CR 36:2.

60. Onomoto K, Onoguchi K, Yoneyama M. 2021. Regulation of RIG-I-like receptor-mediated signaling: interaction between host and viral factors. Cell Mol Immunol 18:539–555.

61. Plociennikowska A, Frankish J, Moraes T, Del Prete D, Kahnt F, Acuna C, Slezak M, Binder M, Bartenschlager R. 2021. TLR3 activation by Zika virus stimulates inflammatory cytokine production which dampens the antiviral response induced by RIG-I-like receptors. J Virol 95:e01050-20, JVI.01050-20.

62. Gashimova NR, Pankratyeva LL, Bitsadze VO, Khizroeva JK, Tretyakova MV, Grigoreva KN, Tsibizova VI, Gris J-C, Degtyareva ND, Yakubova FE, Makatsariya AD. 2023. Inflammation and Immune Reactions in the Fetus as a Response to COVID-19 in the Mother. J Clin Med 12:4256.

63. Jung E, Romero R, Yeo L, Diaz-Primera R, Marin-Concha J, Para R, Lopez AM, Pacora P, Gomez-Lopez N, Yoon BH, Kim CJ, Berry SM, Hsu C-D. 2020. The fetal inflammatory response syndrome: the origins of a concept, pathophysiology, diagnosis, and obstetrical implications. Semin Fetal Neonatal Med 25:101146.

64. Schulze A, Oshi M, Endo I, Takabe K. 2020. MYC Targets Scores Are Associated with Cancer Aggressiveness and Poor Survival in ER-Positive Primary and Metastatic Breast Cancer. Int J Mol Sci 21:8127.

65. Hipfner DR, Cohen SM. 2004. Connecting proliferation and apoptosis in development and disease. Nat Rev Mol Cell Biol 5:805–815.

66. Soares MJ, Iqbal K, Kozai K. 2017. Hypoxia and Placental Development. Birth Defects Res 109:1309–1329.

67. Baker BC, Heazell AEP, Sibley C, Wright R, Bischof H, Beards F, Guevara T, Girard S, Jones RL. 2021. Hypoxia and oxidative stress induce sterile placental inflammation in vitro. Sci Rep 11:7281.

68. Panja S, Paria BC. 2021. Development of the Mouse Placenta. Adv Anat Embryol Cell Biol 234:205–221.

69. Kalluri R, Weinberg RA. 2009. The basics of epithelial-mesenchymal transition. J Clin Invest 119:1420–1428.

70. Marsh B, Blelloch R. 2020. Single nuclei RNA-seq of mouse placental labyrinth development. eLife 9:e60266.

71. Bardot ES, Hadjantonakis A-K. 2020. Mouse gastrulation: Coordination of tissue patterning, specification and diversification of cell fate. Mech Dev 163:103617.

72. Puerta-Guardo H, Glasner DR, Espinosa DA, Biering SB, Patana M, Ratnasiri K, Wang C, Beatty PR, Harris E. 2019. Flavivirus NS1 Triggers Tissue-Specific Vascular Endothelial Dysfunction Reflecting Disease Tropism. Cell Rep 26:1598-1613.e8.

73. Charolidi N, Host AJ, Ashton S, Tryfonos Z, Leslie K, Thilaganathan B, Cartwright JE, Whitley GS. 2019. First trimester placental endothelial cells from pregnancies with abnormal uterine artery Doppler are more sensitive to apoptotic stimuli. Lab Investig J Tech Methods Pathol 99:411–420.

74. Xu S, Ci Y, Wang L, Yang Y, Zhang L, Xu C, Qin C, Shi L. 2019. Zika virus NS3 is a canonical RNA helicase stimulated by NS5 RNA polymerase. Nucleic Acids Res 47:8693–8707.

75. Chen W, Foo S-S, Hong E, Wu C, Lee W-S, Lee S-A, Evseenko D, Moreira MEL, García-Sastre A, Cheng G, Nielsen-Saines K, Brasil P, Avvad-Portari E, Jung JU. 2021. Zika virus NS3 protease induces bone morphogenetic protein-dependent brain calcification in human fetuses. Nat Microbiol 6:455–466.

76. Elong Ngono A, Vizcarra EA, Tang WW, Sheets N, Joo Y, Kim K, Gorman MJ, Diamond MS, Shresta S. 2017. Mapping and Role of the CD8+ T Cell Response During Primary Zika Virus Infection in Mice. Cell Host Microbe 21:35–46.

77. Redline RW, Patterson P. 1993. Villitis of unknown etiology is associated with major infiltration of fetal tissue by maternal inflammatory cells. Am J Pathol 143:473–479.

78. Mahajan S, Alexander A, Koenig Z, Saba N, Prasanphanich N, Hildeman DA, Chougnet CA, DeFranco E, Andorf S, Tilburgs T. 2023. Antigen-specific decidual CD8+ T cells include distinct effector memory and tissue-resident memory cells. JCI Insight 8:e171806.

79. Nazerai L, Schøller AS, Rasmussen POS, Buus S, Stryhn A, Christensen JP, Thomsen AR. 2018. A New In Vivo Model to Study Protective Immunity to Zika Virus Infection in Mice With Intact Type I Interferon Signaling. Front Immunol 9:593.

80. Grifoni A, Costa-Ramos P, Pham J, Tian Y, Rosales SL, Seumois G, Sidney J, de Silva AD, Premkumar L, Collins MH, Stone M, Norris PJ, Romero CME, Durbin A, Ricciardi MJ,

Ledgerwood JE, de Silva AM, Busch M, Peters B, Vijayanand P, Harris E, Falconar AK, Kallas E, Weiskopf D, Sette A. 2018. Cutting Edge: Transcriptional Profiling Reveals Multifunctional and Cytotoxic Antiviral Responses of Zika Virus-Specific CD8+ T Cells. J Immunol Baltim Md 1950 201:3487–3491.

81. Grifoni A, Pham J, Sidney J, O'Rourke PH, Paul S, Peters B, Martini SR, de Silva AD, Ricciardi MJ, Magnani DM, Silveira CGT, Maestri A, Costa PR, de-Oliveira-Pinto LM, de Azeredo EL, Damasco PV, Phillips E, Mallal S, de Silva AM, Collins M, Durbin A, Diehl SA, Cerpas C, Balmaseda A, Kuan G, Coloma J, Harris E, Crowe JE, Stone M, Norris PJ, Busch M, Vivanco-Cid H, Cox J, Graham BS, Ledgerwood JE, Turtle L, Solomon T, Kallas EG, Watkins DI, Weiskopf D, Sette A. 2017. Prior Dengue Virus Exposure Shapes T Cell Immunity to Zika Virus in Humans. J Virol 91:e01469-17.
82. Wen J, Tang WW, Sheets N, Ellison J, Sette A, Kim K, Shresta S. 2017. Identification of Zika virus epitopes reveals immunodominant and protective roles for dengue virus cross-reactive CD8+ T cells. Nat Microbiol 2:17036.
83. Jurado KA, Yockey LJ, Wong PW, Lee S, Huttner AJ, Iwasaki A. 2018. Antiviral CD8 T cells induce Zika-virus-associated paralysis in mice. Nat Microbiol 3:141–147.
84. Grassmann S. 2025. Neonatal T cells unleash innate powers to combat congenital cytomegalovirus infection. J Clin Invest 135:e187789.
85. Elbou Ould MA, Luton D, Yadini M, Pedron B, Aujard Y, Jacqz-Aigrain E, Jacquemard F, Sterkers G. 2004. Cellular immune response of fetuses to cytomegalovirus. Pediatr Res 55:280–286.
86. Tilburgs T, Strominger JL. 2013. CD8+ effector T cells at the fetal-maternal interface, balancing fetal tolerance and antiviral immunity. Am J Reprod Immunol N Y N 1989 69:395–407.
87. Quiñones-Vega M, Velásquez E, Sosa-Acosta P, Melo A, Garcez PP, Nogueira FCS, Domont GB. 2022. Proteomic profiles of Zika virus-infected placentas bearing fetuses with microcephaly. Proteomics Clin Appl 16:e2100042.

88. Clapcote SJ, Roder JC. 2005. Simplex PCR assay for sex determination in mice. BioTechniques 38:702, 704, 706.

89. Jaeger AS, Marano J, Riemersma KK, Castaneda D, Pritchard EM, Pritchard JC, Bohm EK, Baczenas JJ, O'Connor SL, Weger-Lucarelli J, Friedrich TC, Aliota MT. 2023. Gain without pain: adaptation and increased virulence of Zika virus in vertebrate host without fitness cost in mosquito vector. J Virol 97:e0116223.

90. Andrews S. 2010. Babraham bioinformatics - FastQC A quality control tool for high throughput sequence data. http://www.bioinformatics.babraham.ac.uk/projects/fastqc/. Retrieved 16 May 2024.

91. Ewels P, Magnusson M, Lundin S, Käller M. 2016. MultiQC: summarize analysis results for multiple tools and samples in a single report. Bioinformatics 32:3047–3048.

92. Bray NL, Pimentel H, Melsted P, Pachter L. 2016. Near-optimal probabilistic RNA-seq quantification. Nat Biotechnol 34:525–527.

93. Berry ASF, Farias Amorim C, Berry CL, Syrett CM, English ED, Beiting DP. 2021. An Open-Source Toolkit To Expand Bioinformatics Training in Infectious Diseases. MBio 12:e0121421.

94. Soneson C, Love MI, Robinson MD. 2015. Differential analyses for RNA-seq: transcript-level estimates improve gene-level inferences. F1000Res 4:1521.

95. Wickham H. 2009. ggplot2: Elegant Graphics for Data Analysis. Springer Science & Business Media. https://play.google.com/store/books/details?id=bes-AAAAQBAJ.